1970

Traveling wave energy conversion in piezoelectric media

William Henry Childs
Iowa State University

TRAVELING WAVE ENERGY CONVERSION IN PIEZOELECTRIC MEDIA

by

William Henry Childs

A Dissertation Submitted to the

Graduate Faculty in Partial Fulfillment of

The Requirements for the Degree of

DOCTOR OF PHILOSOPHY

Major Subject: Electrical Engineering

Approved:

Signature was redacted for privacy.

In Charge of Major Work

Signature was redacted for privacy.

Head of Major Department

Signature was redacted for privacy.

Dean of Graduate College

Iowa State University
Ames, Iowa

1970

TABLE OF CONTENTS

LIST OF SYMBOLS

stress	-	T_{ij}
strain	-	S_{ij}
stiffness constant at constant D_i	-	c^{D}_{ij}
inverse permittivity at constant S_{ij}	-	β^{S}_{ij}
piezoelectric constant	-	h_{ij}
particle displacement	-	u_i
mass density	-	ρ

I. INTRODUCTION

A. Statement of Problem

This thesis is a theoretical and experimental study of a bulk wave piezoelectric transducer scheme where the transducer regions are defined by strip lines on the piezoelectric crystal. It is intended that they be applied in the microwave frequency range and that the length of the transducer region is to be long with respect to an electrical wavelength.

In particular the concept being considered here envisions a piezoelectric plate of the appropriate symmetry. A ground plane is metalized on one side and strip lines are metalized on the other. Technically these lines would be unshielded microstrip but the dielectric constant of useful piezoelectric materials is so high that it is legitimate to consider them as strip lines. Connection to the outside world will be done in the standard manner via coax to strip line connections. There is obvious flexibility in this scheme and it will be compared to other bulk and surface wave transducers later. It is also a planar scheme with the same production potential as surface wave devices. It is found that certain terminations of the strip line imply a transducer that is not mechanically resonant but still possessing attractive insertion losses. Such a property should facilitate mechanical preparation and also the ability to match the transducer to external circuits. It is also found that certain configurations of these non-mechanically resonant transducers can be located at will on the piezoelectric substrate.

B. Motivation

In the thirteen years since Baranskii (1) and Bommel and Dransfeld (2) reported generation and propagation of acoustic waves in quartz at microwave frequencies, the area of microwave acoustics has grown to the point that special issues of journals (3, 4) are devoted to the topic.

The engineering interest in this field lies primarily in obtaining long time delays in small packages and in various filtering and signal processing schemes. The transducer is obviously a vital component of any microwave acoustic system.

C. Quasi-Static Approximation

Customarily, in analyzing bulk wave transducers, the transducer region is short with respect to an electrical wavelength and an electrical quasi-static approximation can be made (5, 6). That is, it is usual to set $\nabla \times \vec{E} = 0$. In analyzing the proposed transducers, this approximation cannot be made as it is necessary to include $-\mu \partial \vec{H}/\partial t$ to account for the relative length of the transducer region.

Kyame (7, 8) was the first to consider uniform plane wave propagation in a piezoelectric media without making the quasi-static approximation. In a very general way, Kyame considers all the relevant physics of an electromagnetic and acoustic wave traveling through an infinite piezoelectric media. The essential feature of his work is to show that theoretically there are components of the acoustic wave traveling near the electromagnetic velocity and components of the electromagnetic waves traveling near the acoustic velocity. Hutson and White (9) later pointed

out that these waves are negligibly small and that in the typical calculation the quasi-static calculation can always be made.

D. Scope of the Thesis

The general plan of a strip line transducer is to metalize a ground plane on one side of a piezoelectric substrate and strip lines on the other, as indicated in Figure 1. The z axis is intended as the direction of propagation and it will be necessary for the piezoelectric substrate to have the correct symmetry and orientation with respect to the x, y, z coordinate system. For the structures of interest, it will be vital that l be the order of an electrical wavelength, and it is noted that the quasi-static approximation cannot be used in analyzing such a structure.

The class of non-mechanically resonant transducers (which will be termed electrically resonant transducers) will have different terminations than those indicated in Figure 1; the intention here is to indicate what kind of analysis is needed.

If losses in a piezoelectric transducer can be neglected, then all of the power of one form that can be injected into the transducer is converted to power of the other form. Therefore a piezoelectric transducer is properly characterized by its driving point admittances as these will indicate how well it can be matched to the external circuits.

In Chapter II, uniform plane wave (u.p.w.) propagation in a crystal of 4mm (10) symmetry is considered without using the quasi-static approximation. In particular propagation along the c axis and in the basal plane is considered. This constitutes a special direction and symmetry unlike

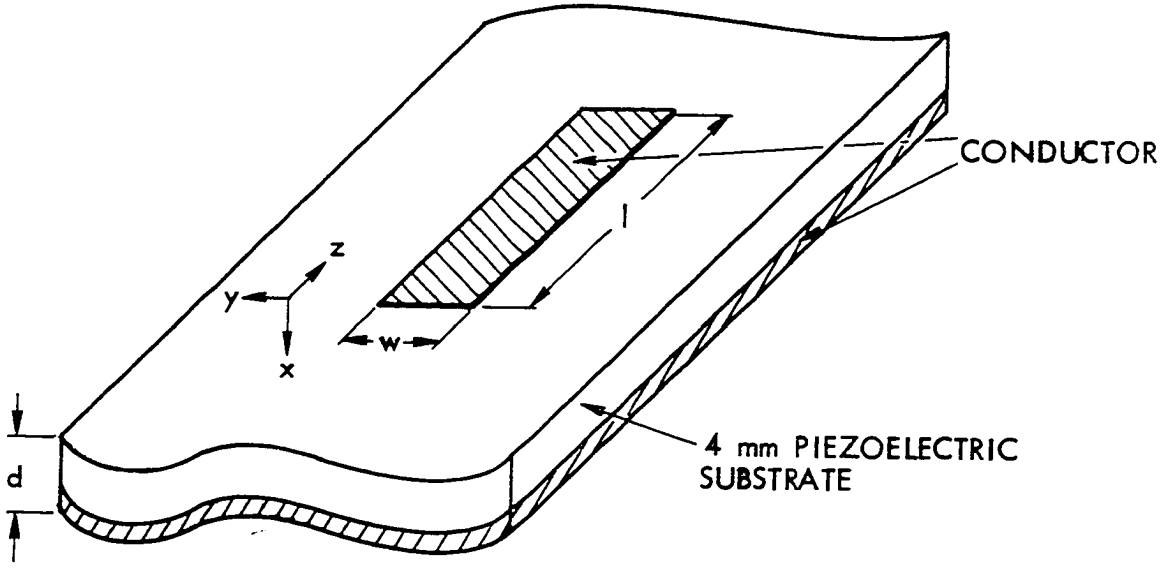

Figure 1. Strip line transducer

Kyame's work (7, 8) that considers a general propagation direction and symmetry. It is found that the waves that result from axis propagation that are appropriate for use in the kind of structure indicated in Figure 1 can be put in a particularly simple one-dimensional model. This one-dimensional model is given a judicious normalization that facilitates later approximation procedures and brings out the analogy to the capacitively coupled transmission line. The static energetics and the significance of Mason's K for these waves is reviewed (11). As is well known (11), K , which is a property of the piezoelectric material, is a measure of goodness of the static energy conversion mechanism. The dynamic power theorem of these waves is reviewed and it is pointed out that the coupling between the acoustic and electromagnetic modes is passive in nature (12). The equations for capacitively coupled transmission lines are indicated and it is seen that the analogy to the non-quasi-static strip line waves is exact. If the coupling, as measured by the piezoelectric constants, goes to zero, one line corresponds to a simple mechanical wave and the other corresponds to a transverse electromagnetic wave. The energy conversion arises through the piezoelectric constants, which are analogous to the coupling capacitors, and the passive transfer (12) or swapping of energy between the two lines that results. If the quasi-static approximation is appropriate, the electrical line is reduced to a capacitor which is capacitively coupled to the acoustic line. The author believes this analogy is original and gives insight to the process of energy conversion in a piezoelectric media.

An exact solution of the strip line waves for the dispersion relation

and wave amplitudes is readily accomplished. As Kyame (7) pointed out, there exist stress and velocity waves traveling near the electromagnetic velocity and electric and magnetic waves traveling near the acoustic velocity. The exact results for the wave amplitudes are not directly interpretable but are made so by an approximation technique that expands all relevant quantities in a power series expansion of $\delta^{n/2}$ where δ is the ratio of the uncoupled acoustic phase velocity to the uncoupled electromagnetic phase velocity and $n = 1,2 \ldots$. This approach is used because it is recognized that even though the static coupling between the two modes could be very strong, the interaction is so highly asynchronous that the dynamic interaction will be very weak and more sensitive to the asynchronism than the coupling. This approximation technique is facilitated by the normalization mentioned earlier. Because δ is so small (typically $\delta \sim 10^{-4}$) only the first terms in each expansion need be kept. The results of this approximation relate the wave amplitudes in a meaningful way. It is found that the electric wave has significant wave amplitudes only at the electric velocity and the velocity wave at the acoustic velocity. The magnetic wave has significant wave amplitudes at the electric velocity and is significantly coupled to the velocity wave and hence has significant wave amplitudes moving at the acoustic velocity. Likewise the stress wave has significant wave amplitudes at the acoustic velocity, but is significantly coupled to the electric wave and hence has significant wave amplitudes moving at the electric velocity. These results are clarified by comparing them to a quasi-static solution of the waves. In the quasi-static approximation, the electric field is a constant and

the magnetic field is the integral of the electric field plus the velocity field times $\sqrt{K\delta}$. The velocity field is just a forward and backward mechanical wave and the stress field is a forward and backward mechanical wave plus the constant electric field times $\sqrt{K\delta}$. If one were trying to modify the quasi-static fields to represent the non-quasi-static case, a good guess would be to let the electric field have a forward and backward component at the electric velocity and substitute this into the above quasi-static fields. Such a procedure is justified by the δ expansion approach which gives the same results. The author believes the δ expansion approach is original in terms of analyzing highly asynchronous problems and that it generates a productive solution for non-quasi-static wave interactions in a piezoelectric.

The non-quasi-static waves are applied to a semi-infinite piezoelectric media where power is injected into the electromagnetic mode at $z = 0$. A fraction of the injected power is periodically swapped between the electromagnetic and acoustic modes and it is shown that this fraction is $4\delta K/\sqrt{1-K}$. The energy conversion mechanism consists of this periodic swapping of energy and the bigger K (the static measure of energy conversion) and the bigger δ then the more energy that is swapped between the modes. It is seen that the dynamic measure of goodness of energy conversion should be considered to be δ .

It is pointed out that if $\lambda_E \gg w \gg d \gg \lambda_A$ where λ_E is the electrical wavelength and λ_A is the acoustic wavelength, then the non-quasi-static uniform plane wave solutions described above can be fitted to the strip line structure indicated in Figure 1. The c axis of the piezoelectric

substrate must be oriented either along the z axis or the x axis. The particular structures of interest (here termed electrically resonant transducers) have the electric field shorted at one or both ends of the strip line. They can be driven electrically in a variety of ways and the practical case of the transducer mechanically terminated in the substrate is considered. The non-quasi-static uniform plane wave solutions described above are applied to this structure. It is found that the boundary condition of a shorted electric field at either end essentially decouples the acoustic and electric transmission lines except for a transformer at the point of electrical excitation. The circuit model so developed can be manipulated to indicate a number of strip line transducers with remarkable properties.

It is found that these shorted strip line transducers when terminated mechanically in the substrate should have no mechanical resonance at all. Essentially this phenomenon arises because the electric field is zero at the point the acoustic wave is launched into the substrate and hence no reflections arise from that point. The way to appreciate this phenomenon is to realize that in a quasi-static transducer there are always (irrespective of the mechanical terminations) mechanical waves moving in both directions in the transducer region. Even if one or both ends of the quasi-static transducer are terminated in an acoustic match, there will still be reflections that can be thought of as arising from the non-zero electric field at the edge of the transducer. The long strip line construction permits one to short the electric field and if the transducer is terminated in an acoustic match, there are no reflections.

The admittance calculations of this kind of transducer imply attractive insertion losses in relation to 50 Ω exciting circuits and practical dimensions of the strip line; in fact the larger K^2, the less the insertion loss. The fact of no mechanical resonance in these structures should greatly facilitate mechanical preparation and external matching. The author knows of no piezoelectric transducer that is not mechanically resonant.

A great drawback to conventional bulk wave microwave frequency transducers is that they must be located on the end of the substrate that the acoustic signal is being stored or manipulated in. In Chapter II it is pointed out that certain configurations of these electrically resonant transducers can be located at will on the substrate. This is a very important property and in strong contrast with quasi-static transducers.

In addition it is noted that the electrically resonant transducer at its electrical resonance presents a real admittance at the point of excitation. This should further facilitate external matching.

In Chapter III the construction and operation of an end excited electrically resonant transducer is described. The transducer was excited by voltage pulses varying in duration from 2ns to 10ns. An acoustical return could be observed for up to 30 μs. It is felt that the details of this acoustical return could be consistently interpreted in terms of the models generated in Chapter II. In Appendix A the dual of the electrically resonant transducer is worked out and this structure has no apparent practical use. Its analysis is included for the sake of completeness. In Appendix B, the strip line transducer is analyzed as if

it were very short with respect to an electrical wavelength and the quasi-static approximation could be employed. This is done just so the results can be compared with the electrically resonant transducer.

E. Comparison to Other Microwave Frequency Transducers

There have been a number of microwave frequency bulk wave transducers invented and perfected. These include quartz bars in insertion cavities with surface excitation of phonons (2), thin quartz bars bonded to the substrate (13), thin magnetic film schemes (14), depletion and diffusion layer transducers (15), and thin piezoelectric film transducers (16). All of these transducers share the property that their location is restricted to the ends of the substrate.

The thin piezoelectric film transducer has been the most successful bulk wave transducer in the sense of gain bandwidth products. These transducers are made by depositing a thin (say one half of an acoustic wavelength for the frequency of interest) film of piezoelectric material on one end of the substrate. The material is usually cadmium sulfide or zinc sulfide. These transducers realize insertion losses comparable to classic transducers built for low frequency (less than 10 MHz) applications (17). They probably constitute the ultimate quasi-static transducer.

The strip line electrically resonant transducer would seem to have a number of advantages over the thin piezoelectric film transducer. Certain configurations of the electrically resonant transducer can be located at will on the substrate. This is an obvious important advantage. The question of gain bandwidth products is difficult to assess because to

compare these transducers practically depends upon the function they are to play, technological achievements in ferroelectric crystals (how long and thin they can be made) which are necessary for the electrically resonant transducers, and how well the E.R.T.'s reactance could be matched by external circuits. The author thinks that the low insertion losses of the thin piezoelectric film transducers will not be equaled by the strip line transducers but the gain bandwidth product will prove to be much larger. The electrically resonant transducer is only practically applied when the piezoelectric transducer region and the substrate are the same. Whether this is an advantage or not depends upon the application and technological achievements in making large ferroelectric crystals. It would appear that, since the electrically resonant transducer has no mechanical resonance, dimensional tolerances in its fabrication will be considerably relaxed and hence high frequency transducers (given the proper piezoelectric substrate) will be readily fabricated. That is, it would appear that they would be considerably easier to fabricate than the thin film transducer. In addition their fabrication is planar in nature.

As a technology, surface wave transducers (18) and devices (19, 20) is probably the direction microwave acoustics applications will follow. Surface wave technology has all the attributes of low insertion loss transducers, flexibility in location of transducers, flexibility in construction of devices, flexibility in the utilization of phonon amplification, and a planar method of construction. The problem facing surface wave technology is the photo mask limit in fabricating devices, which

limits devices made by photo mask techniques to applications below 800 MHz. This limit cannot be pushed higher because of the wavelength of light. Recently 2.5 GHz transducers have been constructed (21) using electron beam fabrication techniques, and it is thought 4.0 GHz operation may be possible. The practicality of this kind of construction remains to be seen.

Strip line transducers share the surface wave transducers' advantages of flexibility in location and planar construction. However a bulk wave is confined to the substrate and cannot be subjected to the kind of manipulation that surface waves can be put to, particularly in utilizing phonon amplification. The strip line electrically resonant transducer would seem to have two advantages over the interdigital electrode transducers used to generate surface waves. Because the electrically resonant transducer is not mechanically resonant, the author thinks that in the long run, the electrically resonant transducer will have more useable bandwidth than any transducer invented to date. This could be particularly useful in memory applications. Secondly, if it proves true that dimensional tolerances can indeed be relaxed because there is no mechanical resonance, then it may be possible to build and use these transducers well above the photo mask limit (800 MHz) that plagues surface wave transducers.

II. ANALYSIS AND APPLICATION OF UNIFORM PLANE WAVE AXIS PROPAGATION IN 4mm PIEZOELECTRIC MATERIALS

A. Formulation of Problem for 4mm Symmetry

The symmetry selected to work in is a 4mm piezoelectric crystal (10). The representation of this symmetry as given by Nye (10) is shown below.

$$\begin{bmatrix} T_{11} \\ T_{22} \\ T_{33} \\ T_{23} \\ T_{13} \\ T_{12} \end{bmatrix} = \begin{bmatrix} C_{11}^{D} & C_{12}^{D} & C_{13}^{D} & 0 & 0 & 0 \\ C_{12}^{D} & C_{11}^{D} & C_{13}^{D} & 0 & 0 & 0 \\ C_{13}^{D} & C_{13}^{D} & C_{33}^{D} & 0 & 0 & 0 \\ 0 & 0 & 0 & C_{44}^{D} & 0 & 0 \\ 0 & 0 & 0 & 0 & C_{44}^{D} & 0 \\ 0 & 0 & 0 & 0 & 0 & C_{66}^{D} \end{bmatrix} \begin{bmatrix} S_{11} \\ S_{22} \\ S_{33} \\ S_{23} \\ S_{13} \\ S_{12} \end{bmatrix}$$

$$- \begin{bmatrix} 0 & 0 & h_{31} \\ 0 & 0 & h_{31} \\ 0 & 0 & h_{33} \\ 0 & h_{15} & 0 \\ h_{15} & 0 & 0 \\ 0 & 0 & 0 \end{bmatrix} \begin{bmatrix} D_1 \\ D_2 \\ D_3 \end{bmatrix} \qquad (1)$$

$$\begin{bmatrix} E_1 \\ E_2 \\ E_3 \end{bmatrix} = \begin{bmatrix} \beta_{11}^S & 0 & 0 \\ 0 & \beta_{11}^S & 0 \\ 0 & 0 & \beta_{33}^S \end{bmatrix} \begin{bmatrix} D_1 \\ D_2 \\ D_3 \end{bmatrix}$$

$$- \begin{bmatrix} 0 & 0 & 0 & 0 & h_{15} & 0 \\ 0 & 0 & 0 & h_{15} & 0 & 0 \\ h_{31} & h_{31} & h_{33} & 0 & 0 & 0 \end{bmatrix} \begin{bmatrix} S_{11} \\ S_{22} \\ S_{33} \\ S_{23} \\ S_{13} \\ S_{12} \end{bmatrix} \tag{2}$$

Engineering strains are used here,

$$S_{ii} = \frac{\partial u_i}{\partial x_i} \tag{3}$$

$$S_{ij} = \frac{\partial u_i}{\partial x_j} + \frac{\partial u_j}{\partial x_i} \tag{4}$$

where u_i is the particle displacement. The force expression is given below.

$$\left[\frac{\partial}{\partial x_1}\ \frac{\partial}{\partial x_2}\ \frac{\partial}{\partial x_3}\right]\begin{bmatrix} T_{11} & T_{12} & T_{13} \\ T_{12} & T_{22} & T_{23} \\ T_{13} & T_{23} & T_{33} \end{bmatrix} = \rho\frac{\partial^2}{\partial t^2}\begin{bmatrix} u_1 \\ u_2 \\ u_3 \end{bmatrix} \tag{5}$$

The formulation is completed with Maxwell's equations.

$$\nabla \times \vec{E} = -\mu\, \partial\vec{H}/\partial t \tag{6}$$

$$\nabla \times \vec{H} = \partial\vec{D}/\partial t \tag{7}$$

$$\nabla \cdot \vec{D} = 0 \tag{8}$$

$$\nabla \cdot \vec{H} = 0 \tag{9}$$

In writing these equations, the following assumptions have been made. It is assumed that 4mm symmetry applies. The conductivity has been assumed to be zero, and it has been assumed there is no free charge. It has been assumed that μ is a constant scalar. The acoustic losses are taken to be negligible. And finally it is implicitly assumed that the macroscopic stress-strain relations are valid at the frequencies of interest.

In this representation, the x_3 direction is the c axis and the x_1,

x_2 plane is the basal plane.

This particular representation with S_{ij} and D_i being the independent variables as opposed to letting T_{ij} and E_i being independent is chosen because the assumption of uniform plane waves causes three of the strains to be zero and one component of the D field to be zero. Considerably more algebraic manipulation is required if T_{ij} and E_i are selected as the independent variables.

B. Basal Plane Propagation

The assumption of uniform plane wave propagation along the x_1 axis is equivalent to assuming uniform plane wave propagation in any direction in the x_1, x_2 plane or basal plane. Therefore, the assumption

$$\frac{\partial}{\partial x_2} = \frac{\partial}{\partial x_3} = 0 \tag{10}$$

is equivalent to assuming arbitrary direction in the basal plane.

As mentioned earlier, the uniform plane wave assumption implies three of the strains are zero. In this case,

$$S_{22} = S_{33} = S_{23} = 0 \tag{11}$$

Also from Equations 8 and 9 it can be concluded that

$$D_1 = H_1 = 0 \tag{12}$$

Substitution of Equations 10-12 into Equations 1, 2 and 5-7 generates the equations which describe basal plane propagation. It is found that these equations can be divided into four independent wave sets which are given below.

$$I_{B.P.}\begin{cases} S_{11} = \partial u_1/\partial x_1 & (13) \\ \partial T_{11}/\partial x_1 = \rho\,\partial^2 u_1/\partial t^2 & (14) \\ T_{11} = c_{11}^D S_{11} - h_{31} D_3 & (15) \\ E_3 = -h_{31} S_{11} + \beta_{33}^S D_3 & (16) \\ \partial E_3/\partial x_1 = \mu\,\partial H_2/\partial t & (17) \\ \partial H_2/\partial x_1 = \partial D_3/\partial t & (18) \\ T_{22} = c_{12}^D S_{11} - h_{31} D_3 & (19) \\ T_{33} = c_{13}^D S_{11} - h_{33} D_3 & (20) \end{cases}$$

$$\text{II}_{\text{B.P.}}\begin{cases} T_{23} = -h_{15}\, D_2 & (21) \\ E_2 = \beta_{11}^{S}\, D_2 & (22) \\ \partial E_2/\partial X_1 = -\mu\, \partial H_3/\partial t & (23) \\ \partial H_3/\partial X_1 = -\partial D_2/\partial t & (24) \\ S_{23} = 0 & (25) \end{cases}$$

$$\text{III}_{\text{B.P.}}\begin{cases} S_{13} = \partial U_3/\partial X_1 & (26) \\ \partial T_{13}/\partial X_1 = \rho\, \partial^2 U_3/\partial t^2 & (27) \\ T_{13} = c_{44}^{D}\, S_{13} & (28) \\ E_1 = -h_{15}\, S_{13} & (29) \end{cases}$$

$$\text{IV}_{\text{B.P.}}\begin{cases} \partial T_{12}/\partial x_1 = \rho\,\partial^2 u_2/\partial t^2 & (30) \\ T_{12} = c_{66}^{D} S_{12} & (31) \\ S_{12} = \partial u_2/\partial x_1 & (32) \end{cases}$$

The Type $\text{IV}_{\text{B.P.}}$ wave is just a mechanical shear wave with no electric coupling. The Type $\text{III}_{\text{B.P.}}$ wave is a shear wave with a longitudinal E field directly coupled to it. The Type $\text{II}_{\text{B.P.}}$ wave is a T.E.M. wave with a shear stress directly coupled to it. The Type $\text{I}_{\text{B.P.}}$ wave is a longitudinal mechanical wave continuously coupled to a T.E.M. wave. The Type $\text{I}_{\text{B.P.}}$ wave will prove to be the solution that is applicable to the proposed strip line structure of Figure 1. In Section M more will be said about fitting this solution to the boundary conditions imposed by the structure of Figure 1. In the future attention will be concentrated on the Type $\text{I}_{\text{B.P.}}$ wave.

C. c Axis Propagation

Uniform plane wave propagation along the c axis is described by letting

$$\partial/\partial x_1 = \partial/\partial x_2 = 0 \qquad (33)$$

This implies

$$S_{11} = S_{22} = S_{12} = 0 \tag{34}$$

and

$$H_3 = D_3 = 0 \tag{35}$$

As before, substitution of Equations 33-35 into Equations 1, 2 and 5-7 generates the equations which describe uniform plane wave propagation along the c axis. It is found that these equations can be divided into three independent wave sets which are given below.

I_c

$$S_{13} = \partial u_1/\partial x_3 \tag{36}$$

$$\partial T_{13}/\partial x_3 = \rho\, \partial^2 u_1/\partial t^2 \tag{37}$$

$$T_{13} = c_{44}^D S_{13} - h_{15} D_1 \tag{38}$$

$$E_1 = \beta_{11}^S D_1 - h_{15} S_{13} \tag{39}$$

$$\partial E_1/\partial x_3 = -\mu\, \partial H_2/\partial t \tag{40}$$

$$\partial H_2/\partial x_3 = -\partial D_1/\partial t \tag{41}$$

$$
\text{II}_c \begin{cases}
S_{23} = \partial u_2/\partial x_3 & (42)\\
\partial T_{23}/\partial x_3 = \rho\, \partial^2 u_2/\partial t^2 & (43)\\
T_{23} = c_{44}^{D} S_{23} - h_{15} D_2 & (44)\\
E_2 = \beta_{11}^{S} D_2 - h_{15} S_{23} & (45)\\
\partial E_2/\partial x_3 = \mu\, \partial H_1/\partial t & (46)\\
\partial H_1/\partial x_3 = \partial D_2/\partial t & (47)
\end{cases}
$$

$$
\text{III}_c \begin{cases}
S_{33} = \partial u_3/\partial x_3 & (48)\\
\partial T_{33}/\partial x_3 = \rho\, \partial^2 u_3/\partial t^2 & (49)\\
T_{33} = c_{33}^{D} S_{33} & (50)\\
T_{22} = c_{13}^{D} S_{33} & (51)\\
T_{11} = c_{13}^{D} S_{33} & (52)\\
E_3 = -h_{33} S_{33} & (53)
\end{cases}
$$

The Type III_c wave is a longitudinal mechanical wave with a longitudinal E field directly coupled to the wave by h_{33}. The Type I_c and II_c waves constitute different polarization of the same wave. The Type I_c or II_c wave is a shear wave that is continuously coupled to a T.E.M. wave. The Type I_c wave will prove to be the solution that is applicable to the proposed strip line structure of Figure 1. In Section M more will be said about fitting this solution to the boundary conditions imposed by the structure of Figure 1. In the future, attention will be concentrated on the Type I_c wave.

D. A One-Dimensional Model of the Type I Waves

A convenient one-dimensional model of the Type I waves is obtained by letting z be the propagation direction and letting the x, y plane be uniform. It is only necessary to consider one polarization of the electromagnetic wave.

$$\partial E_x/\partial z = -\mu\, \partial H_y/\partial t \tag{54}$$

$$\partial H_y/\partial z = -\partial D_x/\partial t \tag{55}$$

The force equation is given by

$$\partial T'/\partial z = -\rho\, \partial^2 u/\partial t^2 \tag{56}$$

where u is the particle displacement and T' is the stress that the particle exerts on the media. The strain is given by

$$S = \partial u / \partial z \tag{57}$$

The equations of state are

$$T' = -\frac{1}{s^D} S + h D_x \tag{58}$$

and

$$E_x = \frac{1}{\epsilon^s} D_x - h S \tag{59}$$

The connection between these one-dimensional variables and the Type I c or basal plane waves is given in Table 1.

It is convenient to reformulate this one-dimensional model in terms of a velocity field,

$$v = \partial u / \partial t \tag{60}$$

Then Equations 54-59 can be put in the form given below.

$$\partial T' / \partial z = -\rho \partial v / \partial t \tag{61}$$

Table 1. Relation of Type $I_{B.P.}$ and I_c waves to the one-dimensional model

One-dimensional Type I wave	Type $I_{B.P.}$ wave	Type I_c wave
z = direction of propagation	x_1 = direction of propagation	x_3 = direction of propagation
S	S_{11}	S_{13}
T'	$-T_{11}$	$-T_{13}$
E_x	$-E_3$	E_1
D_x	$-D_3$	D_1
H_y	H_2	H_2
u	u_1	u_1
$s=1/c^D$	$1/c_{11}^D$	$1/c_{44}^D$
$\epsilon=1/\beta^S$	$1/\beta_{33}^S$	$1/\beta_{11}^S$
$h>0$	$-h_{31}>0$	$h_{15}>0$
$\kappa=h^2\epsilon s$	$\kappa=h_{31}^2/\beta_{33}^S c_{11}^D$	$\kappa=h_{15}^2/\beta_{11}^S c_{44}^D$
$s'=s/1-\kappa$	$\frac{1}{c_{11}^D}\quad\frac{1}{1-\kappa}$	$\frac{1}{c_{44}^D}\quad\frac{1}{1-\kappa}$
$\epsilon'=\epsilon/1-\kappa$	$\frac{1}{\beta_{33}^S}\quad\frac{1}{1-\kappa}$	$\frac{1}{\beta_{11}^S}\quad\frac{1}{1-\kappa}$

$$\partial v/\partial z = -s' \partial T'/\partial t + \frac{1}{h}\frac{\kappa}{1-\kappa}\partial E_x/\partial t \qquad (62)$$

$$\partial H_y/\partial z = -\epsilon' \partial E_x/\partial t + \frac{1}{h}\frac{\kappa}{1-\kappa}\frac{\partial T'}{\partial t} \qquad (63)$$

$$\partial E_x/\partial z = -\mu \partial H_y/\partial t \qquad (64)$$

S and u have been eliminated in favor of v and the following constants have been introduced.

$$\kappa = h^2 \epsilon s \qquad (65)$$

$$\epsilon' = \epsilon/(1-\kappa) \qquad (66)$$

$$s' = s/(1-\kappa) \qquad (67)$$

κ is the well known electromechanical coupling constant generated by Mason (11).

Equations 61-64 are a convenient description of the field interactions that will take place in the strip line transducer. In this description, the quasi-static approximation is made by setting $\mu = 0$

in Equation 64.

E. Normalized Model of Axis Propagation

It is extremely convenient to normalize the dependent variables of Equations 61-64 so that they have the dimensions of the square root of power. The following definitions are necessary.

$$Z'_{AA} = \sqrt{\rho / s'} \tag{68}$$

$$Z'_{EE} = \sqrt{\mu / \epsilon'} \tag{69}$$

$$\beta'_{AA} = \omega\sqrt{\rho s'} = \omega / v'_{AA} \tag{70}$$

$$\beta'_{EE} = \omega\sqrt{\mu\epsilon'} = \omega / v'_{EE} \tag{71}$$

ω is the angular frequency when the time dependence is of the form $\exp(+j\omega t)$.

The dependent variables are normalized as below.

$$\hat{H}_y = \sqrt{Z'_{EE}}\, H_y \tag{72}$$

$$\hat{E}_x = E_x / \sqrt{Z'_{EE}} \tag{73}$$

$$\hat{V} = \sqrt{Z'_{AA}}\, v \tag{74}$$

$$\hat{T}' = T' / \sqrt{Z'_{AA}} \tag{75}$$

These new dependent variables have the following property.

$$S_E = \tfrac{1}{2} E_x H_y^* = \tfrac{1}{2} \hat{E}_x \hat{H}_y^* \tag{76}$$

$$S_A = \tfrac{1}{2} T' V^* = \tfrac{1}{2} \hat{T}' \hat{V}^* \tag{77}$$

Assuming $\exp(+j\omega t)$ time dependence, Equations 61-64 become the following.

$$d\hat{T}'/dz = -j\beta'_{AA} \hat{V} \tag{78}$$

$$d\hat{V}/dz = -j\beta'_{AA} \hat{T}' + j\sqrt{\kappa \beta'_{AA} \beta'_{EE}}\, \hat{E}_x \tag{79}$$

$$d\hat{H}_y/dz = -j\beta'_{EE} \hat{E}_x + j\sqrt{\kappa \beta'_{AA} \beta'_{EE}}\, \hat{T}' \tag{80}$$

$$d\hat{E}_x/dz = -j\beta'_{EE} \hat{H}_y \tag{81}$$

F. Static Energetics of the Axis Piezoelectric Interaction

Mason (11) was the first to point out the significance of the dimensionless quantity $\kappa = h^2/\beta^S c^D$. The author prefers the following interpretation of κ.

The interaction being considered is given in its static one-dimensional form by Equations 58 and 59. These equations can be inverted as below.

$$-S = s' T' - \sqrt{s'\epsilon'\kappa}\, E_x \tag{82}$$

$$D_x = -\sqrt{s'\epsilon'\kappa}\, T' + \epsilon' E_x \tag{83}$$

The energy that is stored in the media by electrical means is

$$\bar{W}_{Elect} = \int_0^D E_x \, dD_x \tag{84}$$

and the energy stored in the media via mechanical means is

$$\bar{W}_{mech} = -\int_0^S T' dS \tag{85}$$

These energies are not state functions (22) but are dependent on the path used to obtain the state D_x, S. However, their sum given by

$$W = \tfrac{1}{2}\epsilon' E_x^2 - \sqrt{s'\epsilon'\kappa}\, E_x T' + \tfrac{1}{2} s' T'^2 \qquad (86)$$

is a state function, here written in terms of the state T', E_x.

It is convenient to make the following definitions.

$$W_E = \tfrac{1}{2}\epsilon' E_x^2 \qquad (87)$$

$$W_m = \tfrac{1}{2} s' T'^2 \qquad (88)$$

$$W_i = \sqrt{s'\epsilon'\kappa}\, E_x T' \qquad (89)$$

$$W = W_E - W_i + W_m \qquad (90)$$

W_E can only be injected or extracted into or out of the media via electrical means. Likewise W_m can only be injected into or extracted from the media via mechanical means. W_i can be injected or extracted electrically or mechanically. W_i is the energy available for conversion. It is observed that

$$\kappa = 1/4\, W_i^2 \Big/ W_E W_m \qquad (91)$$

Therefore, K which is a property of the material, is a measure of goodness for the static energy conversion process in a piezoelectric material for which it can be defined.

G. The Power Theorem for Axis Propagation in a 4mm Piezoelectric

The energy flow in a piezoelectric media is a well understood phenomena (23). Kyame (7) derived a statement of energy flow for the non-quasi-static case. A power theorem is shown here for the simple case of 4mm axis propagation. It is done for the sake of completeness and for the interpretation that would be given to this kind of power theorem in light of coupled mode theory (12).

The statement of energy flow for the traveling wave interaction of Equations 78-81 is obtained in the customary manner. Equations 78 and 79 imply that

$$d\langle S_A\rangle/dz \neq 0 \tag{92}$$

where

$$\langle S_A\rangle = Re\left[\tfrac{1}{2} T' v^*\right] = Re\left[\tfrac{1}{2} \hat{T}' \hat{V}^*\right] \tag{93}$$

$\langle S_A \rangle$ is properly interpreted as the time average acoustic power density. Equations 80 and 81 imply that

$$d\langle S_E\rangle/dz \neq 0 \tag{94}$$

where

$$\langle S_E\rangle = Re\left[\tfrac{1}{2} E_x H_y^*\right] = Re\left[\tfrac{1}{2}\hat{E}_x \hat{H}_y^*\right] \tag{95}$$

$\langle S_E \rangle$ is the time average electromagnetic power density.

If Equations 92 and 94 are added it is found that

$$d\langle S_A\rangle/dz + d\langle S_E\rangle/dz = 0 \tag{96}$$

Equation 96 is a statement of conservation of energy. Equations 92, 94, and 96 together with the form (12) of Equation 78-81 imply that energy is being continuously interchanged between the acoustic mode and the electromagnetic mode as the two modes propagate in the z direction. This type of coupling is called passive mode coupling (12).

H. Capacitively Coupled Transmission Line

Two capacitively coupled transmission lines are shown schematically in Figure 2. The equations that describe such a model are given below with $e^{+j\omega t}$ time dependence having been assumed.

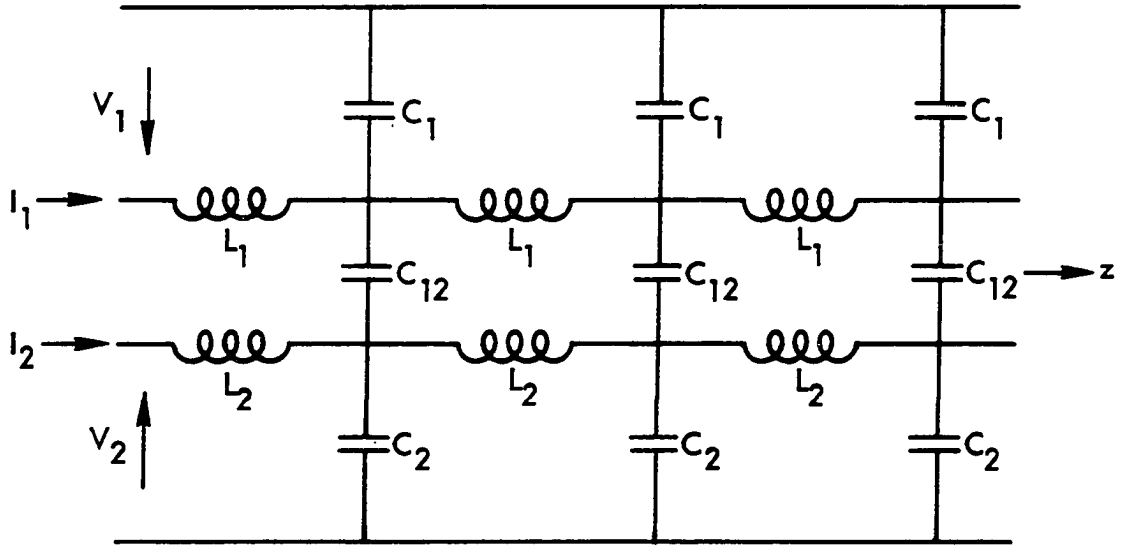

Figure 2. Capacitively coupled transmission line

$$dV_1/dz = -j\omega L_1 I_1 \tag{97}$$

$$dI_1/dz = -j\omega(C_1+C_{12})V_1 + j\omega C_{12}V_2 \tag{98}$$

$$dI_2/dz = -j\omega(C_2+C_{12})V_2 + j\omega C_{12}V_1 \tag{99}$$

$$dV_2/dz = -j\omega L_2 I_2 \tag{100}$$

The following definitions are useful.

$$C_1' = C_1 + C_{12} \tag{101}$$

$$C_2' = C_2 + C_{12} \tag{102}$$

$$Z_1' = \sqrt{L_1/C_1'} \tag{103}$$

$$Z_2' = \sqrt{L_2/C_2'} \tag{104}$$

$$\hat{V}_1(z) = V_1(z)/\sqrt{Z_1'} \tag{105}$$

$$\hat{I}_1(z) = \sqrt{z_1'}\, I_1(z) \tag{106}$$

$$\hat{V}_2(z) = V_2(z) / \sqrt{z_2'} \tag{107}$$

$$\hat{I}_2(z) = \sqrt{z_2'}\, I_2(z) \tag{108}$$

$$\beta_{11}' = \omega \sqrt{L_1 C_1'} \tag{109}$$

$$\beta_{22}' = \omega \sqrt{L_2 C_2'} \tag{110}$$

$$R = C_{12}^2 / C_1' C_2' \tag{111}$$

The dependent variables $\hat{V}_1$, $\hat{I}_1$, $\hat{V}_2$, and $\hat{I}_2$ have the dimensions of the square root of power. In addition,

$$P_1 = \tfrac{1}{2} V_1 I_1^* = \tfrac{1}{2} \hat{V}_1 \hat{I}_1^* \tag{112}$$

and

$$P_2 = \tfrac{1}{2} V_2 I_2^* = \tfrac{1}{2} \hat{V}_2 \hat{I}_2^* \tag{113}$$

Substituting Equations 101-111 into Equation 97-100 implies the following normalized form for the capacitively coupled transmission line.

$$d\hat{V}_1/dz = -j\beta'_{11}\hat{I}_1 \tag{114}$$

$$d\hat{I}_1/dz = -j\beta'_{11}\hat{V}_1 + j\sqrt{R\beta'_{11}\beta'_{22}}\,\hat{V}_2 \tag{115}$$

$$d\hat{I}_2/dz = -j\beta'_{22}\hat{V}_2 + j\sqrt{R\beta'_{11}\beta'_{22}}\,\hat{V}_1 \tag{116}$$

$$d\hat{V}_2/dz = -j\beta'_{22}\hat{I}_2 \tag{117}$$

The analogy between these equations describing two capacitively coupled transmission lines and axis propagation in a 4mm piezoelectric is seen by comparing Equations 78-81 to the above.

In addition it can be seen that R has the same static interpretation as K. If the interaction between the two transmission lines is static then the structure of Figure 2 reduces to the capacitor π network shown in Figure 3. It can be found that the total stored energy in this network is as given below.

$$W = W_1 + W_2 - W_i \tag{118}$$

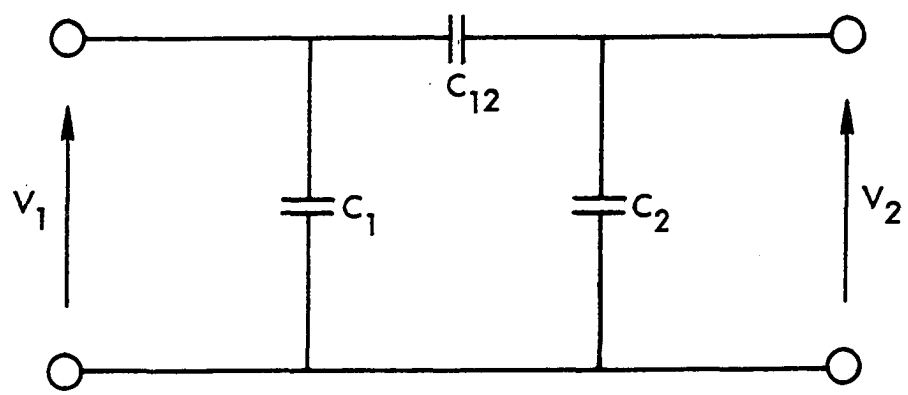

Figure 3. Static interaction between two capacitively coupled transmission lines

$$W_1 = \tfrac{1}{2} C_1' V_1^2 \tag{119}$$

$$W_2 = \tfrac{1}{2} C_2' V_2^2 \tag{120}$$

$$W_i = \sqrt{R C_1' C_2'}\, V_1 V_2 \tag{121}$$

These energies have the same interpretation as the static piezoelectric interaction. W_1 can only be injected or extracted through port 1. Likewise for W_2. W_i can be injected through port 1 and extracted through port 2 or vice-versa. W_i is the energy that can be swapped between the lines on a static basis. Obviously

$$R = \frac{1}{4} \frac{W_i^2}{W_1 W_2} = \frac{C_{12}^2}{C_1' C_2'} \tag{122}$$

R, which is a property of the structure, is a measure of the ability of the structure to swap energy between the lines on a static basis.

The analogy between 4mm axis propagation in a piezoelectric and two capacitively coupled transmission lines is complete.

I. Exact Solution of Axis Propagation in a 4mm Piezoelectric

Axis propagation in a 4mm piezoelectric with a judicious normalization is given by Equations 78-81. Assuming $e^{-j\beta z}$ dependence, the

dispersion relation for these equations is easily found to be prescribed by the following biquadratic equation.

$$(\beta_{AA}^{1/2} - \beta^2)(\beta_{EE}^{1/2} - \beta^2) = \kappa \beta_{AA}^{1/2} \beta_{EE}^{1/2} \tag{123}$$

Equation 123 has the following exact solutions.

$$\beta_A^2 = \frac{1}{2}(\beta_{EE}^{1/2} + \beta_{AA}^{1/2}) + \frac{1}{2}\left[(\beta_{AA}^{1/2} - \beta_{EE}^{1/2})^2 + 4\kappa \beta_{EE}^{1/2} \beta_{AA}^{1/2}\right]^{1/2} \tag{124}$$

$$\beta_E^2 = \frac{1}{2}(\beta_{EE}^{1/2} + \beta_{AA}^{1/2}) - \frac{1}{2}\left[(\beta_{AA}^{1/2} - \beta_{EE}^{1/2})^2 + 4\kappa \beta_{EE}^{1/2} \beta_{AA}^{1/2}\right]^{1/2} \tag{125}$$

The wave amplitudes are found by straightforward algebraic manipulation.

$$\hat{E}_x(z) = \hat{E}^+ e^{-j\beta_E z} - k\sqrt{\frac{\beta'_{EE}}{\beta'_{AA}}}\,\hat{T}^+ e^{-j\beta_A z}$$

$$+ \hat{E}^- e^{+j\beta_E z} - k\sqrt{\frac{\beta'_{EE}}{\beta'_{AA}}}\,\hat{T}^- e^{+j\beta_A z} \qquad (126)$$

$$\hat{H}_y(z) = \frac{\beta_E}{\beta'_{EE}}\,\hat{E}^+ e^{-j\beta_E z} - \frac{k\,\beta_A}{\sqrt{\beta'_{EE}\beta'_{AA}}}\,\hat{T}^+ e^{-j\beta_A z}$$

$$- \frac{\beta_E}{\beta'_{EE}}\,\hat{E}^- e^{+j\beta_E z} + \frac{k\,\beta_A}{\sqrt{\beta'_{EE}\beta'_{AA}}}\,\hat{T}^- e^{+j\beta_A z} \qquad (127)$$

$$\hat{T}'(z) = k\sqrt{\frac{\beta'_{AA}}{\beta'_{EE}}}\,\hat{E}^+ e^{-j\beta_E z} + \hat{T}^+ e^{-j\beta_A z}$$

$$+ k\sqrt{\frac{\beta'_{AA}}{\beta'_{EE}}}\,\hat{E}^- e^{+j\beta_E z} + \hat{T}^- e^{+j\beta_A z} \qquad (128)$$

$$\hat{V}(z) = \frac{k\beta_E}{\sqrt{\beta'_{EE}\beta'_{AA}}}\hat{E}^+ e^{-j\beta_E z} + \frac{\beta_A}{\beta'_{AA}}\hat{T}^+ e^{-j\beta_A z}$$

$$-\frac{k\beta_E}{\sqrt{\beta'_{EE}\beta'_{AA}}}\hat{E}^- e^{+j\beta_E z} - \frac{\beta_A}{\beta'_{AA}}\hat{T}^- e^{+j\beta_A z} \qquad (129)$$

$$k^2 = \frac{\beta_A^2 - \beta_{AA}'^2}{\beta_{AA}'^2 - \beta_E^2}$$

$$= \frac{\beta_{EE}'^2 - \beta_E^2}{\beta_A^2 - \beta_{EE}'^2} \qquad (130)$$

As mentioned earlier in discussing Kyame's work (7), the non-quasi-static solution of this interaction predicts a component of the electromagnetic wave moving at the acoustic velocity and a component of the mechanical wave moving at the electrical velocity. The perturbation technique below will clarify the significance of these amplitudes and relate them to the quasi-static approximation.

J. Approximate Solution of Axis Propagation in a 4mm Piezoelectric Media

To make the above exact solution more meaningful, the exact solutions are expanded in a power series

$$\delta^{n/2} \qquad n = 1, 2, 3 \cdots \tag{131}$$

where

$$\delta = \frac{\beta'_{EE}}{\beta'_{AA}} = \frac{v'_{AA}}{v'_{EE}} \tag{132}$$

and it is assumed that $\delta << 1$. The motivation for doing this is the fact that for nearly synchronous interactions between two wave systems, it is found (12, 24) that the strength of the interaction depends on the synchronism and the strength of coupling. This interaction is highly asynchronous ($\delta \sim 10^{-3}$ to 10^{-4}) and one might suspect the degree of asynchronism is the major factor in relating the wave amplitudes. As will be seen below, this is a very good approximation and only the first term in each expansion need be kept.

Applying this procedure to the dispersion relation given by Equations 124 and 125, it is found that

$$\beta_A^2 = \beta_{AA}'^2 \left[1 + \kappa \delta^2 + \theta(\delta^4) + \cdots \right] \tag{133}$$

and

$$\beta_E^2 = \beta_{EE}'^2 \left[(1-\kappa) - \kappa\delta^2(1-\kappa) + \Theta(\delta^4) + \cdots\right] \tag{134}$$

where Θ means order of. Obviously it is a good approximation to let

$$\beta_A^2 \cong \beta_{AA}'^2 + \Theta(\delta^2) \tag{135}$$

and

$$\beta_E^2 \cong \beta_{EE}'^2 (1-\kappa) + \Theta(\delta^2) \tag{136}$$

The constant k is approximated as above by using Equations 133 and 134 in Equation 130. It is found that

$$k \cong \sqrt{\kappa}\,\delta + \Theta(\delta^2) \tag{137}$$

The exact wave amplitudes of Equations 126-129 are rewritten in terms of

$$\hat{E}_x(z) = \hat{E}^+ e^{-j\beta_E z} - \sqrt{\delta}\, k\, \hat{T}^+ e^{-j\beta_A z} + \text{b.w.} \tag{138}$$

$$\hat{H}_y(z) = \frac{\beta_E}{\beta'_{EE}} \hat{E}^+ e^{-j\beta_E z} - \sqrt{\delta}\, k \frac{\beta_A}{\beta'_{EE}} \hat{T}^+ e^{-j\beta_A z} + \text{b.w.} \tag{139}$$

$$\hat{T}'(z) = \frac{k}{\sqrt{\delta}} \hat{E}^+ e^{-j\beta_E z} + \hat{T}^+ e^{-j\beta_A z} + \text{b.w.} \tag{140}$$

$$\hat{V}(z) = \frac{k}{\sqrt{\delta}} \frac{\beta_E}{\beta'_{AA}} \hat{E}^+ e^{-j\beta_E z} + \frac{\beta_A}{\beta'_{AA}} \hat{T}^+ e^{-j\beta_A z} + \text{b.w.} \tag{141}$$

The abbreviation, b.w., stands for the backward waves.

Then substituting freely from Equations 133-135 implies the following results for the wave amplitudes.

$$\sqrt{\delta}\, k = \sqrt{\kappa}\, \delta^{3/2} + \Theta(\delta^{5/2}) \tag{142}$$

$$\beta_E / \beta'_{EE} = \sqrt{1-\kappa}\,\left(1 + \Theta(\delta^2)\right) \tag{143}$$

$$k\sqrt{\delta}\,\beta_A / \beta'_{EE} = \sqrt{\delta\kappa} + \Theta(\delta^{3/2}) \tag{144}$$

$$k/\sqrt{\delta} = \sqrt{\delta\kappa} + \Theta(\delta^{3/2}) \tag{145}$$

$$\frac{k}{\sqrt{\delta}}\,\frac{\beta_E}{\beta'_{AA}} = \sqrt{1-\kappa}\sqrt{\kappa}\,\delta^{3/2} + \Theta(\delta^{5/2}) \tag{146}$$

$$\frac{\beta_A}{\beta'_{AA}} = 1 + \Theta(\delta^2) \tag{147}$$

δ will be so small that the wave amplitudes are approximated through order δ as below.

$$\hat{E}_x(z) = \hat{E}^+ e^{-j\beta_E z} + \hat{E}^- e^{+j\beta_E z} \tag{148}$$

$$\hat{H}_y(z) = \sqrt{1-\kappa}\,\hat{E}^+ e^{-j\beta_E z} - \sqrt{\delta\kappa}\,\hat{T}^+ e^{-j\beta_A z}$$
$$- \sqrt{1-\kappa}\,\hat{E}^- e^{+j\beta_E z} + \sqrt{\delta\kappa}\,\hat{T}^- e^{+j\beta_A z} \qquad (149)$$

$$\hat{T}'(z) = \sqrt{\delta\kappa}\,\hat{E}^+ e^{-j\beta_E z} + \hat{T}^+ e^{-j\beta_A z}$$
$$+ \sqrt{\delta\kappa}\,\hat{E}^- e^{+j\beta_E z} + \hat{T}^- e^{+j\beta_A z} \qquad (150)$$

$$\hat{V}(z) = \hat{T}^+ e^{-j\beta_A z} - \hat{T}^- e^{+j\beta_A z} \qquad (151)$$

These results show that only the magnetic field has a significant component moving at the acoustic velocity and only the stress field has a significant component moving at the electromagnetic velocity. The similar components of the electric field and velocity field are much smaller in relation to the above components and can safely be ignored. The wave amplitudes as prescribed by Equations 148-151 are the ones

that will be used in future calculations.

K. Relation of the Approximate Traveling Wave Solutions to the Quasi-Static Approximation

The greatest bulk of acoustic work is done using the quasi-static approximation. In particular when the interaction region of the transducer is small with respect to an electrical wavelength, it is a good approximation to set the right hand side of Equation 81 to zero. If Equations 78-81 are solved with the electric field assumed to be constant, then the exact results are as below.

$$\hat{V}(z) = \hat{T}^{+} e^{-j\beta'_{AA} z} - \hat{T}^{-} e^{+j\beta'_{AA} z} \tag{152}$$

$$\hat{T}'(z) = \hat{T}^{+} e^{-j\beta'_{AA} z} + \hat{T}^{-} e^{+j\beta'_{AA} z} + \sqrt{Ks}\,\hat{E}_x \tag{153}$$

$$\hat{H}_y(z) = -j\beta'_{EE} \int \hat{E}_x\, dz - \sqrt{Ks}\,\hat{T}^{+} e^{-j\beta'_{AA} z} + \sqrt{Ks}\,\hat{T}^{-} e^{+j\beta'_{AA} z} \tag{154}$$

$$\hat{E}_x = \text{constant} \tag{155}$$

If the interaction region is of significant length with respect to an electrical wavelength, then the electric field cannot be approximated as a constant. A good guess as how the above quasi-static results should be modified in such a case would be

$$\hat{E}_x = \hat{E}^+ e^{-j\beta_E z} + \hat{E}^- e^{+j\beta_E z} \tag{156}$$

Substitution of Equation 156 into Equations 152-155 gives Equations 149-151. The more precise approximation procedure of Section J justifies the above modification of the quasi-static results.

L. Power Transfer on the Semi-Infinite Structure

It is interesting to consider the situation where the media is terminated at z = 0 in a stress free surface and the boundary conditions are such that $\langle S_{inj} \rangle$ watts/meter^2 are injected into the electromagnetic mode. It is assumed the media extends to infinity.

The semi-infinite structure assumption implies that there are no backward waves. The stress free assumption at z = 0 implies

$$\hat{T}^+ = -\sqrt{\delta\kappa}\,\hat{E}^+ \tag{157}$$

Substitution of Equation 157 into Equations 148-151 gives the waves on this structure as below.

$$\hat{E}_x = \hat{E}^+ e^{-j\beta_E z} \tag{158}$$

$$\hat{H}_y = \sqrt{1-\kappa}\,\hat{E}^+ e^{-j\beta_E z} + \delta\kappa\,\hat{E}^+ e^{-j\beta_A z} \tag{159}$$

$$T' = \sqrt{\delta\kappa}\,\hat{E}^+ \left(e^{-j\beta_E z} - e^{-j\beta_A z}\right) \tag{160}$$

$$\hat{V} = -\sqrt{\delta\kappa}\,\hat{E}^+ e^{-j\beta_A z} \tag{161}$$

The energy flow in this structure is given below.

$$\left\langle \tfrac{1}{2}\hat{E}_x \hat{H}_y^* \right\rangle = \langle S_{inj} \rangle \left[1 - \frac{4\delta\kappa}{\sqrt{1-\kappa}} \sin^2\left(\frac{\beta_A - \beta_E}{2}\right) z\right] \tag{162}$$

$$\left\langle \tfrac{1}{2}\hat{T}'\hat{V}^* \right\rangle = \langle S_{inj} \rangle \frac{4\delta\kappa}{\sqrt{1-\kappa}} \sin^2\left(\frac{\beta_A - \beta_E}{2}\right) z \tag{163}$$

It is seen that energy is periodically swapped between the acoustic and electromagnetic modes. The fraction that is transferred is proportional to δ and depends on K. The dependence on K is such that the larger K the larger the fraction of injected power that can be transferred to the acoustic mode. K and its role in the static energy conversion process have been discussed earlier in Section F. Equations 162 and 163 imply that the dynamic energy conversion process is also measured by K but also depends on the asynchronism given by δ. These results are similar to other traveling wave interactions in which it is typically found that the stronger the coupling and the higher the degree of synchronism, the more pronounced the interaction between the coupled wave systems. It is noted that there is no quasi-static analogue for the problem considered here.

M. Electrically Resonant Transducer

In this section, a transducer scheme that is electrically resonant but not mechanically resonant is analyzed. However this particular structure has a similar insertion loss to structures that are mechanically resonant. Fabrication tolerances and external matching problems should be considerably relaxed over mechanically resonant devices.

In the preceding sections, uniform plane wave propagation along the axes of a 4mm piezoelectric material was investigated. The intention is to analyze strip line transducers as generally indicated in Figure 1. It is thought that the waves represented by the one-dimensional model of Section D meet the boundary conditions of the strip line structure in-

dicated in Figure 1 with the following provisos:

$$\lambda_E \gg W \tag{164}$$

where λ_E is the electrical wavelength,

$$\frac{W}{d} \gg 1 \tag{165}$$

and

$$d \gg \lambda_A \tag{166}$$

where λ_A is the acoustic wavelength. It is felt that if the above inequalities are met, the assumption of uniform variations in the x, y plane will be met. It is intended that the z axis is the direction of wave propagation. In order to coincide with the directions of propagation investigated in previous sections, the c axis must be either oriented in the z direction or the x direction. The former case will be called a c axis transducer and the latter a basal plane transducer. For the particular devices of interest, it will be vital that 1 be the order of an electrical wavelength. Specific implementations of the electrically resonant transducer which will be analyzed below are discussed in the following sections. The intention here is to outline the restrictions (Equations 164-166) for which it is thought the fields represented by the previous uniform plane analysis meet the boundary

conditions imposed by the strip line structure shown in Figure 1.

The electrically resonant transducer (E.R.T.) is shown schematically in Figures 4a and 4b. The dual of the circuit shown in Figure 4 is one that is clamped at $z = \pm l_{\pm}$. Since there is no apparent practical application for such a structure, its analysis is carried out in Appendix 1.

Without specifying the excitation at z = 0, the boundary conditions for the structure shown in Figure 4 are given below.

$$\hat{E}_x(-l_-) = 0 \tag{167}$$

$$\hat{E}_x(l_+) = 0 \tag{168}$$

$$\hat{V}(0^-) = \hat{V}(0^+) \tag{169}$$

$$\hat{I}'(0^-) = \hat{I}'(0^+) \tag{170}$$

Applying Equations 167 and 168 to Equations 148-151 implies the following.

$$\hat{E}_x(z) = \hat{E}_x(0^{\mp}) \frac{\sin\beta_E(l_{\mp} \pm z)}{\sin\beta_E l_{\mp}} \tag{171}$$

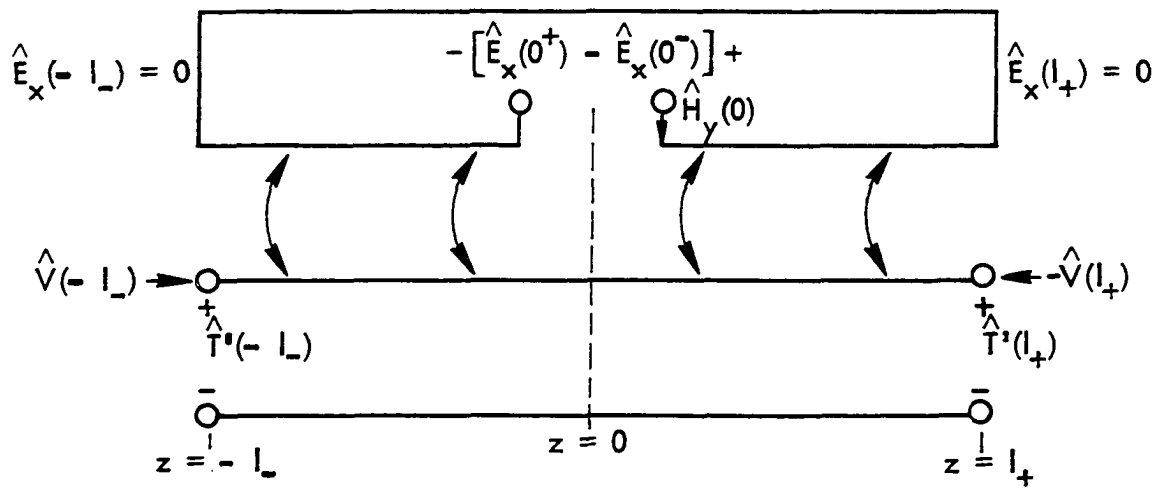

Figure 4a. The electrically resonant transducer with balanced excitation

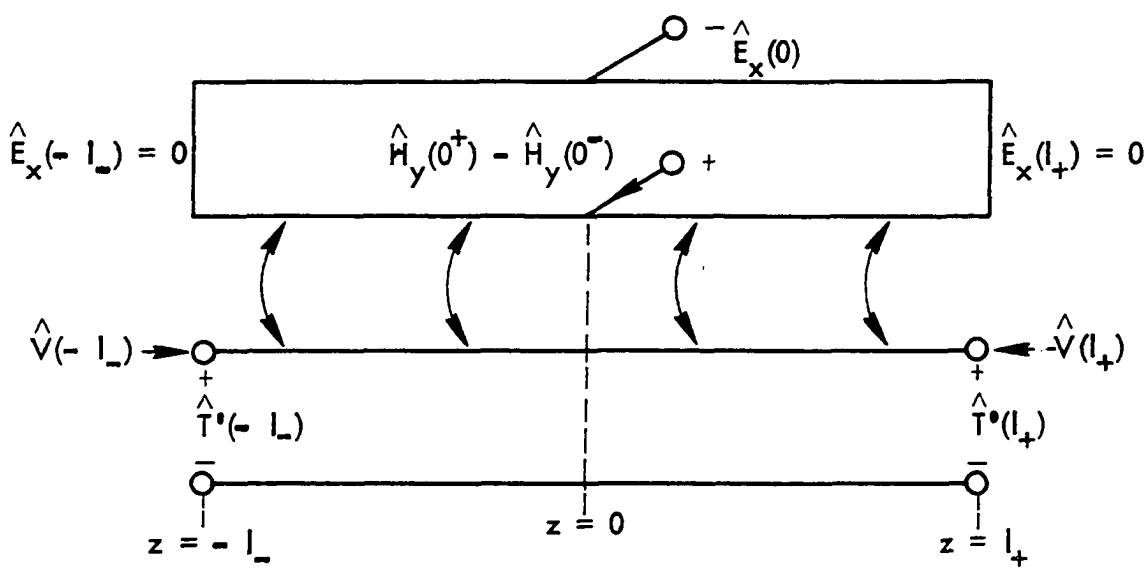

Figure 4b. The electrically resonant transducer with unbalanced excitation

$$\hat{H}_y(z) = \pm j\sqrt{1-\kappa}\,\hat{E}_x(0^{\mp})\frac{\cos\beta_E(l_{\mp} \pm z)}{\sin\beta_E l_{\mp}} - \sqrt{\kappa\delta}\,\hat{V}(z) \tag{172}$$

$$\hat{T}'(z) = \sqrt{\kappa\delta}\,\hat{E}_x(z) + \hat{T}^{+}_{\mp} e^{-j\beta_A z} + \hat{T}^{-}_{\mp} e^{+j\beta_A z} \tag{173}$$

$$\hat{V}(z) = \hat{T}^{+}_{\mp} e^{-j\beta_A z} - \hat{T}^{-}_{\mp} e^{+j\beta_A z} \tag{174}$$

The top sign is to be applied for $z < 0$ and the bottom sign for $z > 0$.

It is useful to define the following variables.

$$\hat{h} = \hat{H}_y + \sqrt{\kappa\delta}\,\hat{V} = \pm j\sqrt{1-\kappa}\,\hat{E}_x(0^{\mp})\frac{\cos\beta_E(l_{\mp} \pm z)}{\sin\beta_E l_{\mp}} \tag{175}$$

$$\hat{\mathcal{T}} = \hat{T}' - \sqrt{\kappa s}\,\hat{E}_x$$

$$= \hat{T}^+_{\mp}\, e^{-j\beta_A z} + \hat{T}^-_{\mp}\, e^{+j\beta_A z} \qquad (176)$$

It is observed that

$$\hat{\mathcal{T}}(\mp l_{\mp}) = \hat{T}'(\mp l_{\mp}) \qquad (177)$$

because of the boundary condition imposed there. It is seen from Equations 174 and 176 that $\hat{t}$ and $\hat{v}$ are the standard transmission line variables. $\hat{\mathcal{T}}$ is useful because it is equal to the real stress, T', at the outside world, $z = \mp l_{\mp}$ as given by Equation 177.

From Equation 170 and 176, it can be concluded that

$$\hat{\mathcal{T}}(0^+) - \hat{\mathcal{T}}(0^-) = -\sqrt{\kappa s}\left[\hat{E}_x(0^+) - \hat{E}_x(0^-)\right] \qquad (178)$$

Therefore it can be seen that if the excitation is unbalanced ($\hat{E}_x(0^+) = \hat{E}_x(0^-)$) both $\hat{t}$ and $\hat{v}$ will be continuous at z = 0 and the mechanical line will be uncoupled from the electrical line. Therefore unbalanced excitation at z = 0 leads to no interaction between the acoustic and electromagnetic modes and will not be considered further.

Balanced excitation as shown in Figure 4a is considered.

$$\hat{H}_y(0^-) = \hat{H}_y(0^+) = \hat{H}_y(0) \tag{179}$$

Because both $\hat{v}$ and $\hat{H}_y$ are continuous,

$$\hat{h}(0^-) = \hat{h}(0^+) = \hat{h}(0) \tag{180}$$

Then

$$\hat{H}_y(0) = \hat{h}(0) - \sqrt{\kappa\delta}\,\hat{V}(0) \tag{181}$$

Using Equations 181 and 178, it is found that

$$\frac{\hat{H}_y(0)}{\hat{E}_x(0^+) - \hat{E}_x(0^-)} = \frac{\hat{h}(0) - \sqrt{\kappa\delta}\,\hat{V}(0)}{\hat{E}_x(0^+) - \hat{E}_x(0^-)}$$

$$= \frac{\hat{h}(0)}{\hat{E}_x(0^+) - \hat{E}_x(0^-)} + \frac{\kappa\delta\,\hat{V}(0)}{\hat{f}(0^+) - \hat{f}(0^-)} \tag{182}$$

$$= \frac{1}{\left(\frac{\hat{E}_x(0^+)}{\hat{h}(0)}\right) + \left(-\frac{\hat{E}_x(0^-)}{\hat{h}(0)}\right)} - \frac{\kappa\delta}{\left(\frac{\hat{f}(0^-)}{\hat{V}(0)} + \left(-\frac{\hat{f}(0^+)}{\hat{V}(0)}\right)\right.}$$

Equations 178, 181, and 182 are conveniently represented by the circuit model shown in Figure 5.

Equation 175 gives

(183)

The quantities $\hat{t}\ (0\ \mp)/\hat{v}(0)$ are related to the quantities $\hat{T}'(\mp l_{\mp})/\hat{V}(\mp l_{\mp})$ by the standard transmission line translations which are given below.

$$\pm \frac{\hat{I}(0^{\mp})}{\hat{V}(0)} =$$

$$= \frac{1 + e^{-2j\beta A l_{\mp}}\left[\dfrac{\mp\hat{T}'(\mp l_{\mp})/\hat{V}(\mp l_{\mp}) - 1}{\mp\hat{T}'(\mp l_{\mp})/\hat{V}(\mp l_{\mp}) + 1}\right]}{1 - e^{-2j\beta A l_{\mp}}\left[\dfrac{\mp\hat{T}'(\mp l_{\mp})/\hat{V}(\mp l_{\mp}) - 1}{\mp\hat{T}'(\mp l_{\mp})/\hat{V}(\mp l_{\mp}) + 1}\right]} \qquad (184)$$

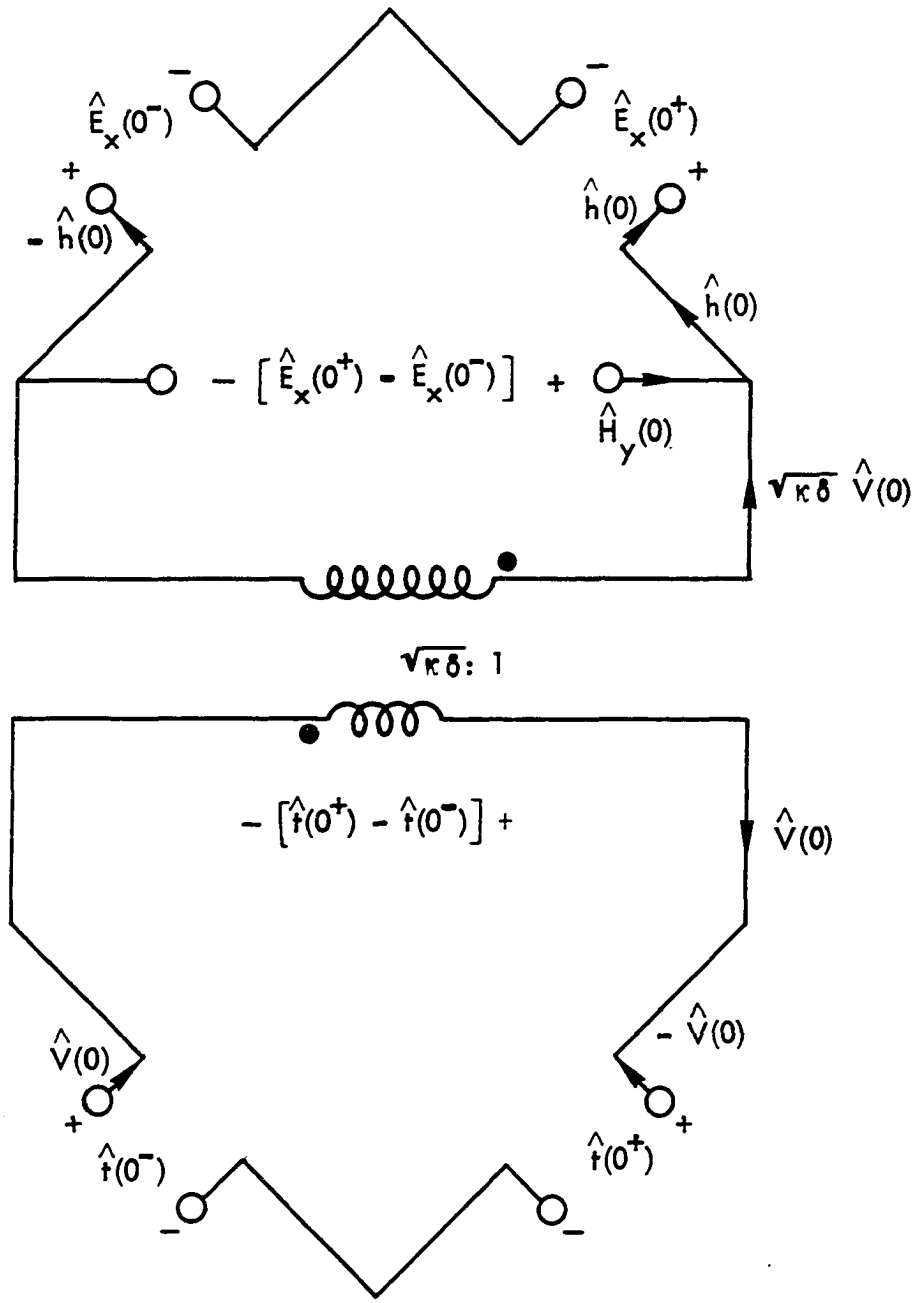

Figure 5. Circuit showing relation of variables at z = 0 for E.R.T. with balanced excitation

$$\pm \frac{\hat{T}'(\mp l_{\mp})}{\hat{V}(\mp l_{\mp})} =$$

$$\frac{1 + e^{-2j\beta_A l_{\mp}}\left[\dfrac{\pm \hat{I}(0^{\mp})/\hat{V}(0) - 1}{\pm \hat{I}(0^{\mp})/\hat{V}(0) + 1}\right]}{1 - e^{-2j\beta_A l_{\mp}}\left[\dfrac{\pm \hat{I}(0^{\mp})/\hat{V}(0) - 1}{\pm \hat{I}(0^{\mp})/\hat{V}(0) + 1}\right]} \qquad (185)$$

The circuit model of Figure 5 is expanded by using Equations 183-185 as shown in Figure 6. The model of Figure 6 properly relates the three accessible ports in the structure of Figure 4a. The actual behavior of $\hat{T}'$ and $\hat{H}_y$ everywhere in the structure of Figure 4a is given by the above equations. However the relationship among the three accessible ports is described by the model of Figure 6 whose validity is established by the above equations. The essential feature of the model in Figure 6 is the way the mechanical and electrical modes can be regarded as uncoupled except for the transformer located at the point of excitation. As pointed out earlier, this decoupling occurs because the electric field was forced to be zero at $z = \pm l_{\pm}$. In essence the E.R.T. structure of Figure 4a and as modeled in Figure 6 can be regarded as a balanced electrical source in parallel with two series connected stubs and transformer coupled to a

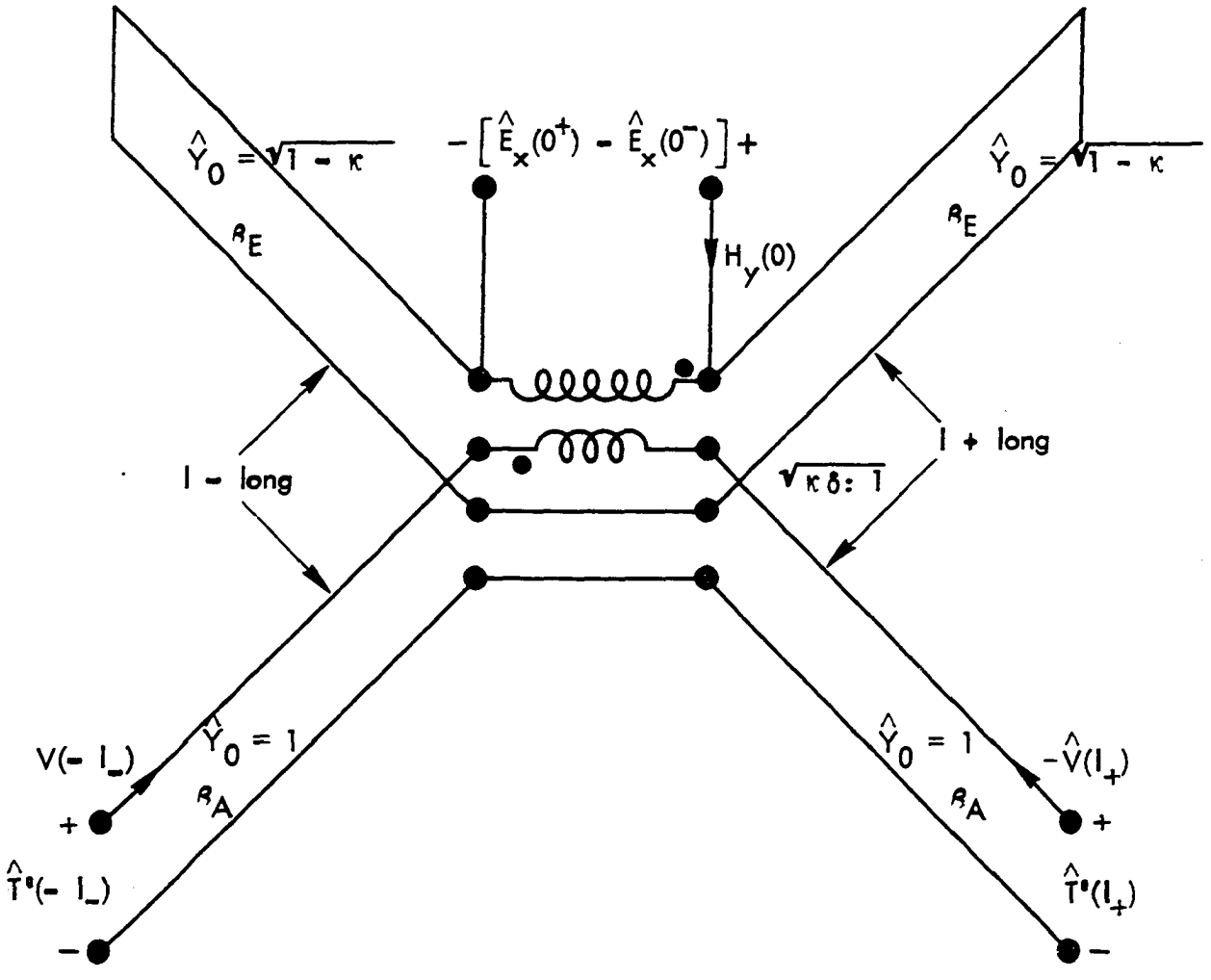

Figure 6. Model showing behavior of E.R.T. at its accessible parts

mechanical transmission line of length l_- in one direction and l_+ in the other.

It should be noted that there is no non-trivial quasi-static analogue to the structure considered in Figure 4a and modeled in Figure 6. The quasi-static limit of the E.R.T. would consist of a shorted electric field at the point of excitation and hence no coupling to the mechanical mode at all. Practical implementations of the E.R.T. are considered in the next three sections.

N. E.R.T. Located on the End of a Stress Free Bar

The E.R.T. situated on the end of a stress free bar is shown schematically in Figure 7. The circuit model of this device as deduced from the more general model of Section M, Figure 6, is shown in Figure 8. An idealization of a physical realization of this structure is shown in Figure 9. It is intended that Figure 9 be a sideview with the width of the device being w. It is assumed that the bond at $z = l$ is perfect. This structure would meet the boundary conditions exactly. A possible practical implementation of this structure is shown in Figure 10. It is thought that the manner in which the electric field is shorted at $z = l$ will not disturb the T.E.M. nature of the fields there significantly. The structure being considered here shares the property of typical quasi-static devices in that its location is fixed at the end of the bar. In the next two sections, transducers that can be located arbitrarily on the substrate are considered.

The practical case where the transducer is terminated in its own

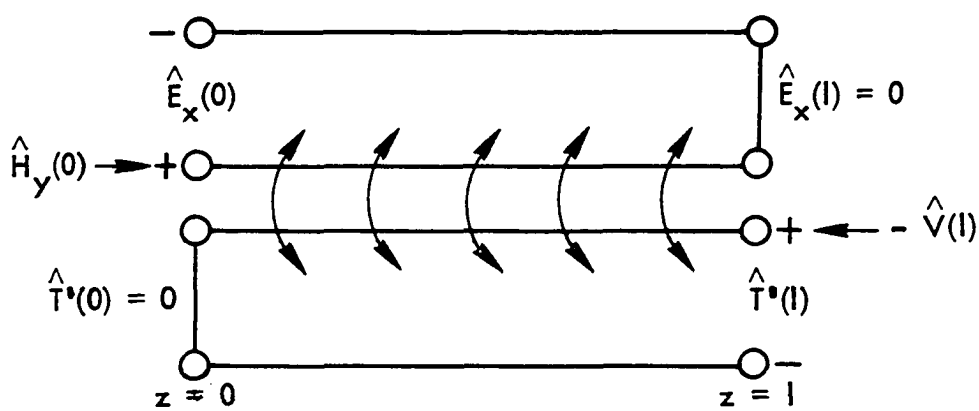

Figure 7. Schematic representation of the E.R.T. on the end of a stress free bar

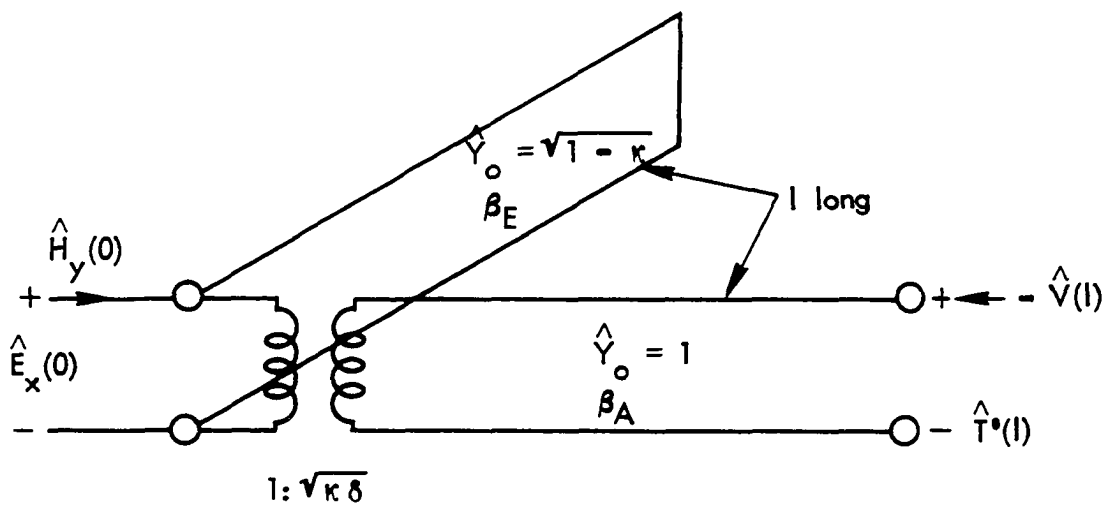

Figure 8. Model showing relation between accessible ports of the E.R.T. when located on the end of a stress free bar

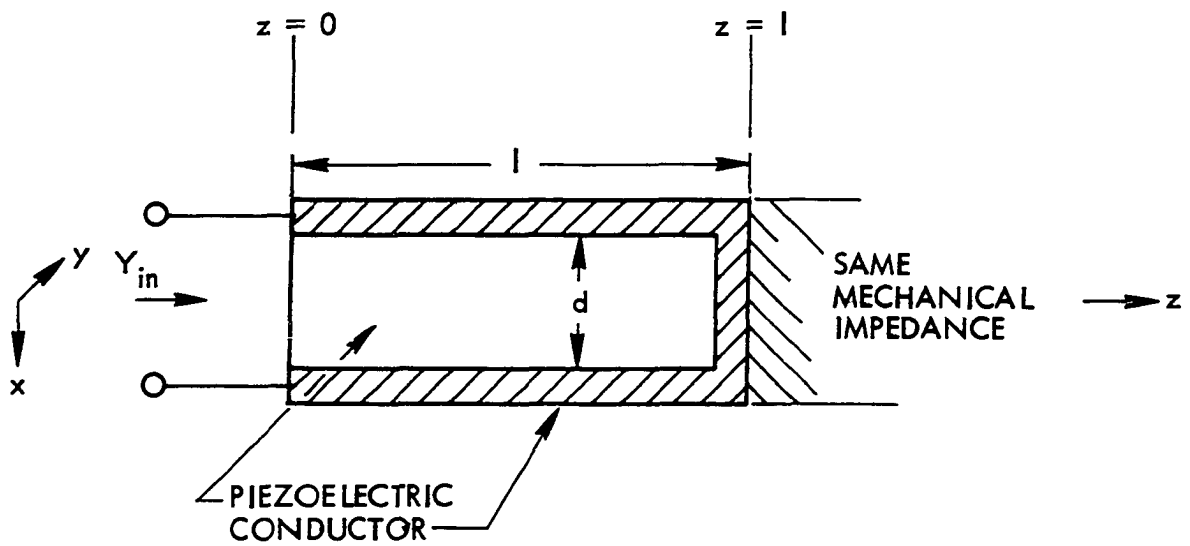

Figure 9. Physical idealization of the electrically resonant transducer on the end of a stress free bar

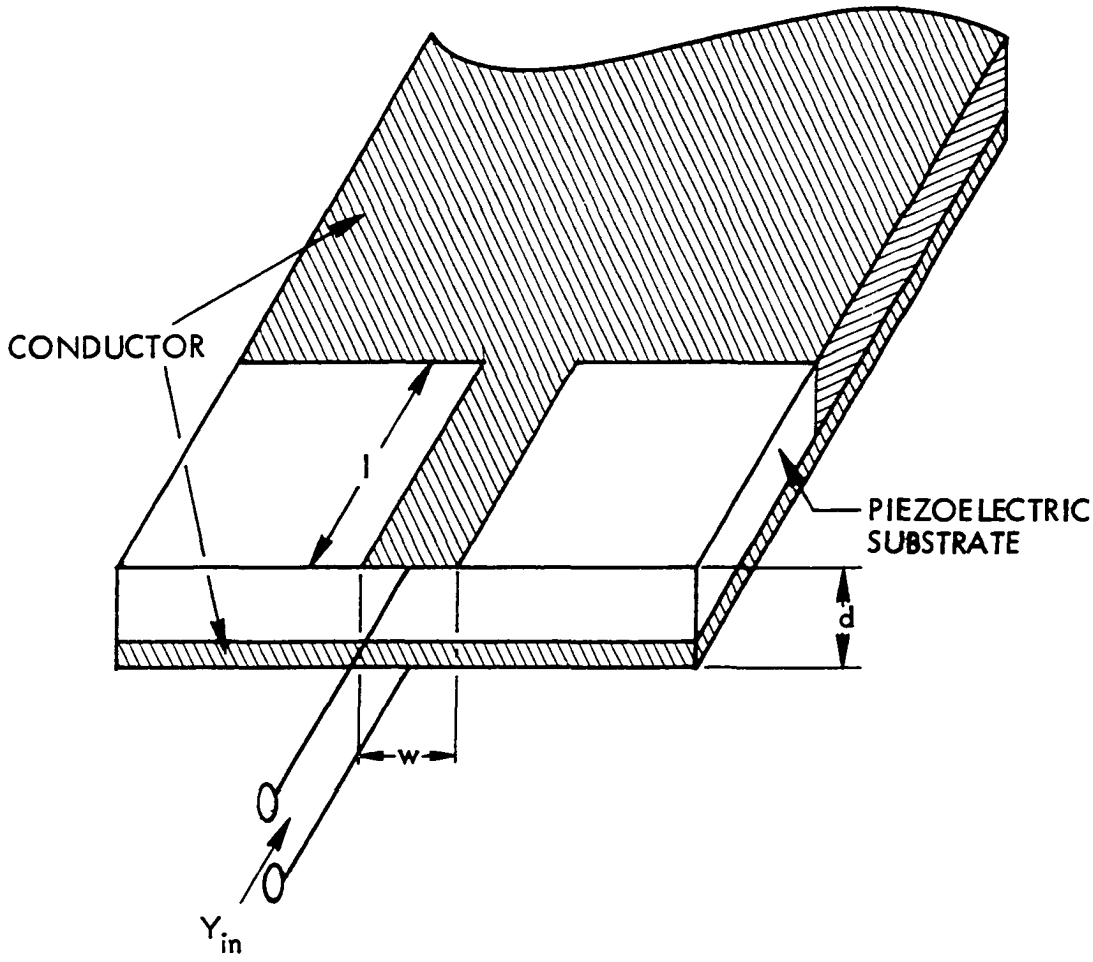

Figure 10. Possible physical realization on the electrically resonant transducer on the end of a stress free bar

mechanical impedance as shown in Figure 10 is considered.

$$\hat{T}'(\ell) = \hat{V}(\ell) \tag{186}$$

It is apparent then from the circuit model of Figure 8 that

$$\hat{H}_y(0)/\hat{E}_x(0) = \hat{Y}_{inE} = -j\sqrt{1-K^2}\cot\beta_E\ell + \delta K \tag{187}$$

When the transducer is terminated in its match impedance, the electrical driving point admittance is not dependent on a mechanical resonance. Within the transducer region there is only a mechanical wave moving in the + z direction and not the - z direction. This remarkable property comes about because the electric field is shorted at z = 1 and doesn't cause a reflection as it does in quasi-static devices. In addition, it is noted that when the structure is in a quarter wave electrical resonance, the driving point admittance is real.

$$\hat{Y}_{inE}\Big|_{\ell=\frac{\lambda_E}{4}} = \left.\frac{\hat{H}_y(0)}{\hat{E}_x(0)}\right|_{\ell=\lambda_E/4} = \delta K \tag{188}$$

This is a property of the strip line transducer that the quasi-static device doesn't have. At an electrical resonance, the strip line transducer presents a real admittance and there is no need to tune out a

reactance in the external matching circuitry.

The actual driving point admittance of the structure is given below (25).

$$Y_{inE} = \frac{W}{d} \frac{1}{Z'_{EE}} \hat{Y}_{inE} \tag{189}$$

When the structure is at a quarter wave electrical resonance,

$$\hat{Y}_{inE}\Big|_{\ell=\lambda_E/4} = \frac{W}{d}\sqrt{\frac{\epsilon_0}{\mu_0}}\sqrt{\frac{\epsilon'}{\epsilon_0}}\,\delta K \tag{190}$$

As seen in Appendix B, this result is entirely comparable to a similar quasi-static device at mechanical resonance. To facilitate matching, it is desirable that the quantity $\delta K\sqrt{\epsilon'/\epsilon_0}$ be as large as possible. This suggests that a ferroelectric material be used as the piezoelectric substrate because of the extremely high permittivities that can be found in some ferroelectrics (26-28). The parameters that have previously been found important for axis propagation in a 4mm piezoelectric are shown for the case of barium titanate in Table 2. This data is based on the single crystal measurements of Berlincourt and Jaffe (29). Using this data in Table 2, it is found that

$$Y_{inE}\Big|_{\ell=\lambda_E/4} = \frac{1}{50\Omega}\left(1.25\times10^{-3}\frac{W}{d}\right) \tag{191}$$

Table 2. Pertinent constants for axis propagation in $BaTiO_3$

Values from the one dimensional mode	Propagation in the basal plane	Propagation along the c axis
ρ	$6020 kg/m^3$	$6020 kg/m^3$
s	$3.54 \times 10^{-12} m^2/N$	$12.4 \times 10^{-12} m^2/N$
ϵ	$112 \epsilon_o$	$1970 \epsilon_o$
h	$-.269 \times 10^{10} V/m$	$.122 \times 10^{10} V/m$
κ	.0254	.322
s'	$3.63 \times 10^{-12} m^2/N$	$18.3 \times 10^{-12} m^2/N$
ϵ'	$115 \epsilon_o$	$2920 \epsilon_o$
$v_A \sim v_{A'A}$	$6.78 \times 10^3 m/s$	$3.01 \times 10^3 m/s$
$v_{E'E}$	$2.8 \times 10^7 m/s$	$5.56 \times 10^6 m/s$
v_E	$2.83 \times 10^7 m/s$	$6.76 \times 10^6 m/s$
δ	$.242 \times 10^{-3}$	$.542 \times 10^{-3}$
$\delta\kappa$	$.615 \times 10^{-5}$	1.74×10^{-4}
$\sqrt{\epsilon'/\epsilon_o}\,\delta\kappa$	$.658 \times 10^{-4}$	$.94 \times 10^{-2}$
$1/v'_{AA}$	1.48 μ s/cm	3.32 μ s/cm

for propagation along the c axis and

$$Y_{inE}\Big|_{l=\lambda_E/4} = \frac{1}{50\Omega}\left(.87\times10^{-5}\frac{W}{d}\right) \qquad (192)$$

for propagation in the basal plane.

Transducers are generally characterized by their insertion loss. It is supposed that Y_o is the characteristic admittance of the external exciting circuit. The definition

$$\hat{Y}_o = \frac{d}{W} Z'_{EE} Y_o \qquad (193)$$

is made. Only the situation at electrical resonance, $l = \lambda_E/4$, is considered. Then

$$\Gamma_{inE} = \frac{\hat{Y}_o - \delta K}{\hat{Y}_o + \delta K} \qquad (194)$$

In considering the case where mechanical energy is converted to electrical, it is assumed that

$$-\hat{H}_y(0)/\hat{E}_x(0) = \hat{Y}_o + j\sqrt{1-K}\cot\beta_E l \qquad (195)$$

then

$$\Gamma_{inA} = \frac{\delta K - \hat{Y}_0}{\delta K + \hat{Y}_0} \tag{196}$$

Define

$$|\Gamma_{in}|^2 = |\Gamma_{inE}|^2 = |\Gamma_{inA}|^2 \tag{197}$$

Then

$$\begin{aligned} I.L. &= \text{Insertion Loss} \\ &= -10 \log_{10}[1 - |\Gamma_{in}|^2]\, dB \\ &= -10 \log_{10}\left[\frac{4\delta K \hat{Y}_0}{(\delta K + \hat{Y}_0)^2}\right] dB \end{aligned} \tag{198}$$

For a modest aspect ration of w/d = 10 and $Y_0 = 1/50\Omega$, it is found that for a c axis $BaTiO_3$ transducer $I.L. \sim 13dB$ and for a basal plane $BaTiO_3$ transducer $I.L. \sim 35dB$.

O. Arbitrarily Located End Excited E.R.T.

In the last section, the transducer scheme analyzed was confined to the end of the substrate in order to meet the stress free assumption. In this section, an E.R.T. is proposed that should be capable of arbitrary location on the piezoelectric substrate. A schematic representation of

this transducer is shown in Figure 11. The model of the port behavior as deduced from the model of Section M, Figure 6, is shown in Figure 12. A possible physical realization of this transducer is shown in Figure 13. Here again it is supposed that the manner in which the electric field is shorted at z = l, will not disturb the T.E.M. nature of the fields there.

The practical case where the transducer is terminated in its own match impedance is considered.

$$\hat{V}(l)/\hat{T}'(l) = 1 \tag{199}$$

$$-\hat{V}(0)/\hat{T}'(0) = 1 \tag{200}$$

Then from Figure 12, it can be deduced that

$$\hat{Y}_{IME} = \frac{\hat{H}_y(0)}{\hat{E}_x(0)} = -j\sqrt{1-\kappa}\cot\beta_E l + \tfrac{1}{2}\delta\kappa \tag{201}$$

This is entirely similar to the admittance calculated in Section N except that the real part of the admittance is decreased by a factor of two.

The calculation of insertion loss proceeds in the same fashion as in Section N and it is found that

$$I.L. = -10\log_{10}\left[\frac{2Y_0\,\delta\kappa/2}{(\tfrac{1}{2}\delta\kappa + \hat{Y}_0)^2}\right] dB \tag{202}$$

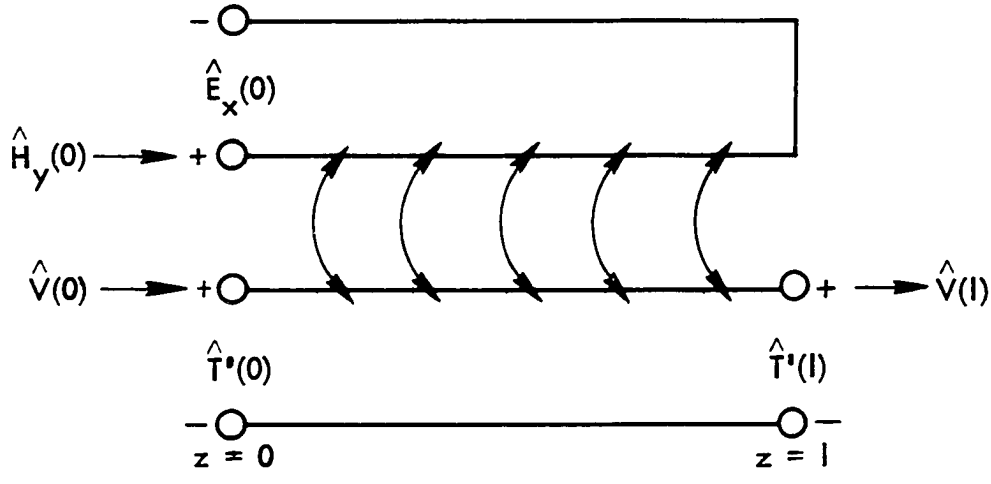

Figure 11. Schematic representation of the E.R.T. arbitrarily located on the piezoelectric substrate with end excitation

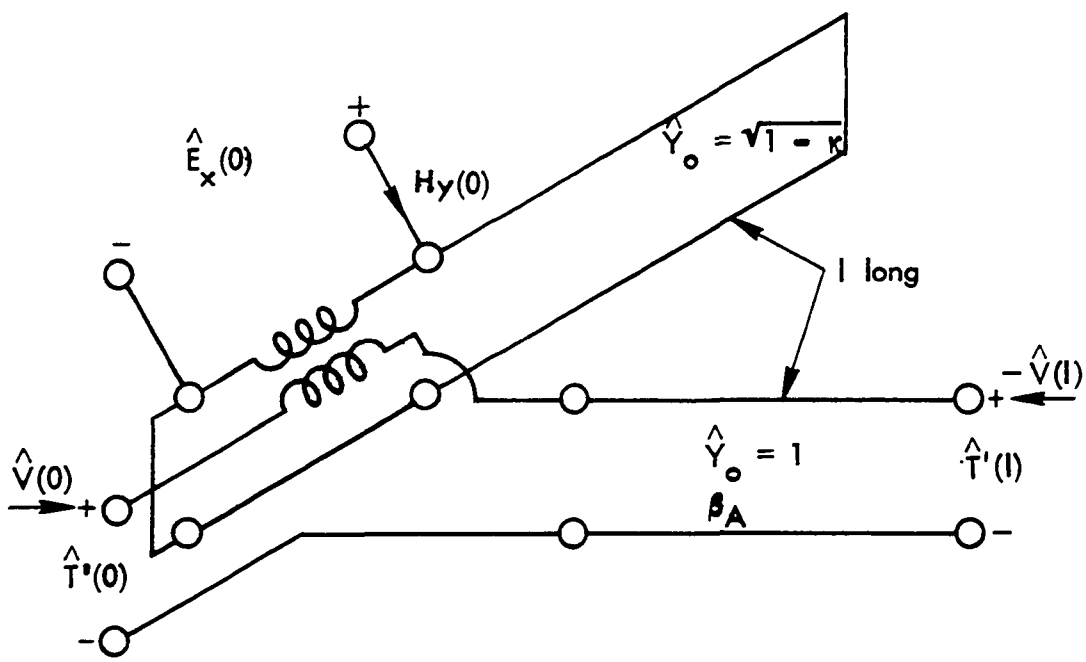

Figure 12. Model showing relation between accessible ports of the arbitrarily located end excited E.R.T.

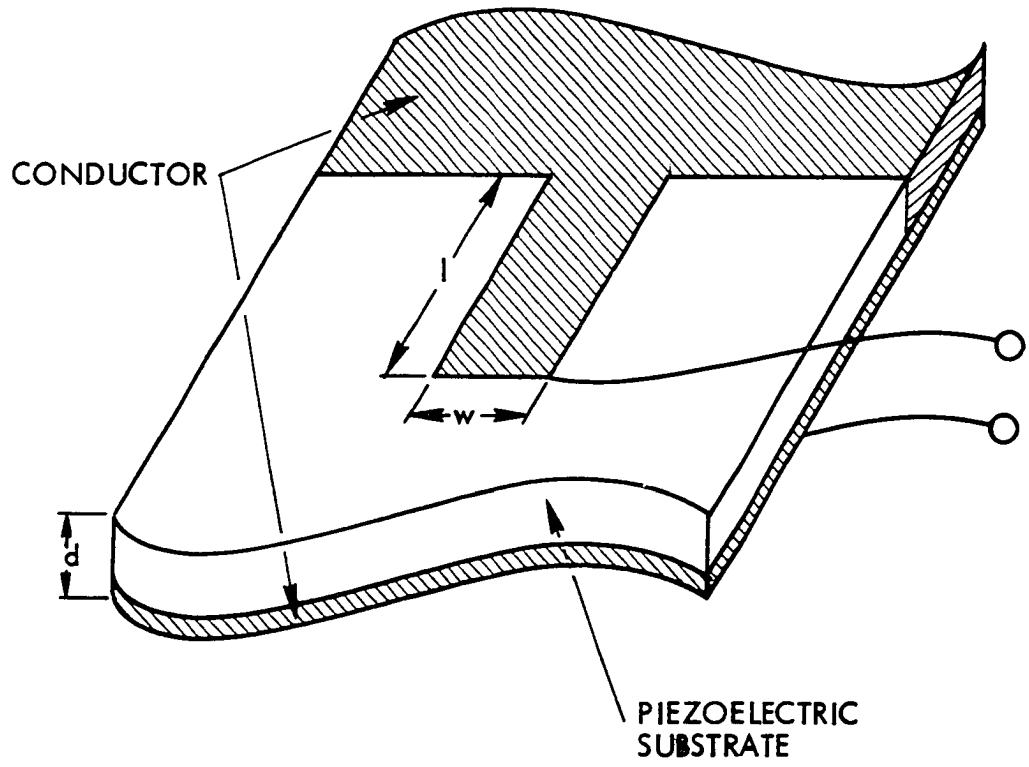

Figure 13. Possible physical realization of the arbitrarily located end excited E.R.T.

where $\hat{Y}_o$ is given by Equation 193. It is observed that even if the external electrical exciting circuit could be exactly matched to the transducer ($\hat{Y}_o = \delta K/2$) there would still be 3dB of loss. This is because half of the acoustic power will be launched in the - z direction and half in the + z direction and only one direction is considered useful. Likewise when a mechanical wave is incident upon the transducer, some of the power (half if $\hat{Y}_o = \delta K/2$) will be converted into electrical energy and some lost into the substrate on the other side of the transducer. These facts are taken into account in Equation 202.

Using the data given in Table 2 and and assuming w/d = 10 and $Y_o = 1/50\ \Omega$, it is found using Equation 202 that I.L. ~ 19dB for a c axis $BaTiO_3$ transducer and I.L. ~ 41dB for a basal plane $BaTiO_3$ transducer.

P. Arbitrarily Located E.R.T. with Balanced Excitation

The transducer scheme discussed here is just the realization of the general E.R.T. model discussed in Section M. This transducer is schematically indicated in Figure 4a and the circuit model is shown in Figure 6. The practical case of matched terminations in the acoustic line is considered. A possible physical realization of this structure is shown in Figure 14. It is intended that the exciting line be metalized on the substrate along with the strip line and that it be magnetically coupled to the strip line as indicated. The characterization of the coupling between the exciting line and the strip line will not be considered here

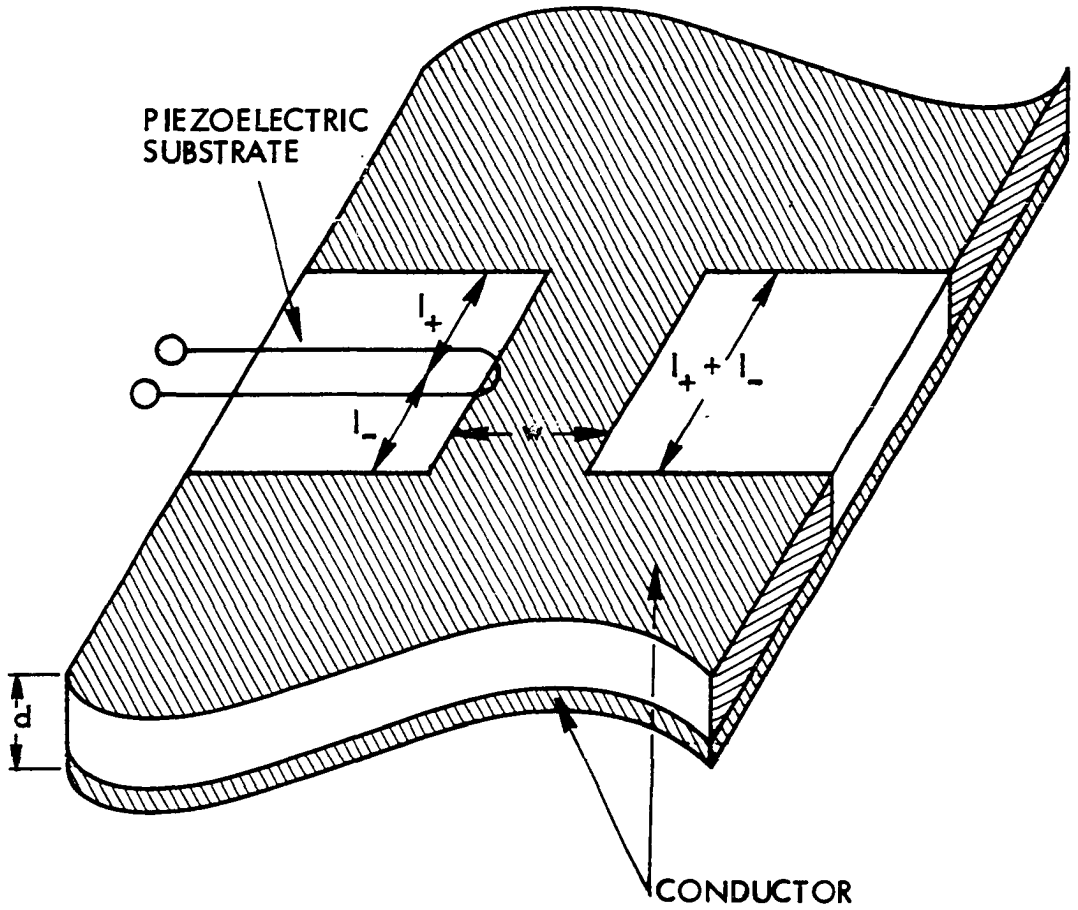

Figure 14. Possible physical realization of the arbitrarily located E.R.T. with balanced excitation

and the characterization of the driving point admittance will be done as if the strip line were excited as shown in Figure 4a.

The transducer scheme proposed here can also be arbitrarily located on the substrate. The only difference between this scheme and the one discussed in Section 0 is that midpoint balanced excitation is used here. It is apparent from the circuit model of Figure 6, that there is no mechanical resonance in this structure and that either stub can be resonated to tune out the reactance presented at the electrical port. That is, resonance corresponds to either $l_+ = \lambda_E/4$ or $l_- = \lambda_E/4$.

Considering an electrical source at $z = 0$ and the acoustic lines matched at $z = \pm l_\pm$, the physical situation in the transducer is the following: For $z > 0$ there is one mechanical wave moving in the + z direction and for $z < 0$ there is one mechanical wave moving in the - z direction. Equal amounts of power are delivered to the match loads at $z = \pm l_\pm$. Considering a mechanical wave incident on the transducer from $z > l_+$ moving in the - z direction, the physical situation in the transducer is the following: Part of the - z directed wave is transmitted on through the transducer, part is converted to electrical energy and extracted through the electrical port, and part is reflected back down the line to the port at $z = l_+$. If the port at $z = -l_-$ is matched, there is only a mechanical wave moving in the - z direction for $-l_- < Z < 0$ and the reflection in $0 < z < l_+$ can be thought of as being caused by the electrical load at $z = 0$.

Equation 202 is to be used in calculating the resonant insertion loss of this structure and the same numerical estimates of insertion loss for a $BaTiO_3$ substrate stated in Section 0 can be applied here.

III. EXPERIMENTAL PROGRAM

A. Introductory Comments

As pointed out in Chapter II, the practical implementation of the strip line transducer depends on being able to use ferroelectric crystals. Barium titanate ($BaTiO_3$) was chosen as the experimental material because fairly large crystals of this material were available and the properties of this material as reported in the literature (26, 27, 28, 29, 30, 31) were deemed desirable. $BaTiO_3$ is grown in plates with one of the nominal cubic axes (30, 31) perpendicular to the plate. If large enough crystals could be consistently obtained, $BaTiO_3$ would appear to be a good choice for use as the substrate in devices utilizing the proposed strip line transducers.

Also, as pointed out in Chapter II, if $BaTiO_3$ is to be used as the substrate, then the c axis mode of operation is very desirable compared to the basal plane mode. In fact the calculations for insertion loss when c axis propagation is used can be termed attractive. The difficulty in building a c axis transducer is that it appears that the single "a" domain (30, 31) must be formed prior to the metalization of the strip line. Difficulties were encountered in carrying this process to completion. Instead basal plane transducers were constructed because they could be metalized and the single "c" domain (30, 31) then formed.

It would be desirable to form the strip lines on the substrate using photo mask techniques (32). The effect of subjecting the $BaTiO_3$ to the etchant was unknown and it was decided to directly mask the crystal and

then metalize the strip lines. This is a crude technique and it will undoubtedly become necessary to find a material that photo mask techniques can be used upon.

The experiment reported here involves bouncing a very short duration pulse off the end of a bar. The bars were carefully cut on a wire saw, but no polishing of the ends was attempted. Good $B_aT_iO_3$ crystals are fairly flat, and extensive etching in phosphoric acid above the Curie temperature seems to make them very flat (33). The transducer scheme considered in this thesis envisions two or more transducers placed on the substrate, and the problem of polishing the ends of the transducer in order to observe a bounce would be of no importance. A bounce experiment was performed here because overly large crystals were not available and this in essence doubled the available delay.

The experiment reported here excited the basal plane mode in a shorted strip line transducer with a short duration (2ns - 10ns) voltage pulse. The author feels that the observed acoustical returns are strong evidence that the analysis and models of Chapter II are correct.

B. Transducer Fabrication

Several different strip line transducers were constructed and tested. The intention here is to describe a successful one in terms of available crystals and success in fabrication and testing.

A large, fairly defect-free, single crystal of $BaTiO_3$ was selected. The crystal was observed through crossed polarizers and the nominal cubic axes in the plate of crystal noted. The crystal was carefully cut on a

wire saw. It was cut into a bar with its edges parallel to the nominal cubic axes with dimensions 1.14cm x .28cm x .028cm. The bar was cleaned in various organic solvents and given a brief etch in phosphoric acid heated to 140° C.

The bar was then mounted on a mask using silicone grease. The grease was applied in such a way that it would not be in the path of the acoustic beam as generated by the strip line. Aluminum was evaporated onto the bar to form a ground plane on one side and to form on the other side a .125cm strip running the length of the bar and roughly centered in that face. The thickness of this evaporation was estimated to be 3500Å.

The bar was then bonded ground plane down onto another ground plane which was part of a jig. The jig accomplishes the coaxial to strip line transition. The bond was accomplished with conducting silver paint. About 1 cm of copper wire was soldered to a round silver electrode, .234cm in diameter. The electrode was bonded by silver paint to one end of the strip line. The other end of the wire was attached to the center lead of the coaxial cable. The outer shield of the coaxial cable was attached to the ground plane. This coax to strip line transition is rather crude, but reliable. The transition was accomplished in such a short distance with respect to wavelengths of interest that it is thought to be valid in the sense of interpreting experimental results with respect to the preceding analysis. Investigation of the transition with a time domain reflectometer indicated negligible reflections due to the transition.

The device was then cooled to -15°C and 200V applied to the strip line for an estimated field strength of approximately 7kV/cm. The device was slowly warmed to 27°C and the electric field removed. The author has found this to be a more reliable way to accomplish single "c" domains than the usual technique of heating the crystal above the Curie temperature. Experiments with removable electrodes indicate a high probability that single "c" domains will be obtained in this fashion. The metalization on the device being described here prevents one from observing the domains through crossed polarizers, but the experimental results discussed below indicate that a single "c" domain is indeed obtained.

The electrical short at the end of the strip line was obtained by painting the end of the bar with conducting silver paint.

C. Transducer Testing

It is thought that the transducer whose fabrication is described above is properly modeled by the end excited E.R.T. shown in Figure 12. The right hand end of the acoustic line in Figure 12 is shorted (stress free surface) and the left hand acoustic line extends a short distance to the left and is terminated in a short also.

Referring to Table 2, it is found that the electrical line has a very low wave impedance (approximately 1 Ω) and the acoustic line (as seen through the transformer) has a very high impedance (approximately $10^5\,\Omega$). Elementary considerations show that a voltage spike incident on the transducer from a 50 Ω system will reappear after the acoustic delay with approximately 10^{-6} of its initial value. The transducer

of length 1.14cm described in Section B should have a total electrical delay of approximately 1ns and a total acoustic delay of approximately 3.4ms based on the data in Table 2.

The electrical observations were carried out in the following manner. A 50Ω pulse generator drove the midpoint of a tee. One side of the tee was connected to the transducer with about 20cm of 50Ω cable. The other side of the tee was connected to an amplifier with approximately 80dB of gain and 8MHz of bandwidth. The center frequency of the amplifier was 30MHz. The output of the amplifier was observed on an oscilloscope with 85MHz of bandwidth. The amplifier had the ability to recover quickly when greatly overdriven. That is, the initial voltage pulse did not noticeably saturate the amplifier in looking for returns after this pulse was finished.

Figure 15 is an observation of the reflection of a 2ns pulse from the beginning of the transducer. The second negative notch is probably the reflection from the short at the end of the transducer. The photograph in Figure 15 was made on a sampling oscilloscope without use of the amplifier described above.

Figures 16-19 are photographs of the output of the amplifier as observed on an 85MHz oscilloscope. They were all taken with the amplifier having about 80dB of power gain. Figures 16-18 are for a pulse repetition frequency of 50kHz and Figure 19 of 20kHz. The initial voltage pulse in all four figures had an amplitude of 4V. The vertical scaling in these figures is 100mV/cm and the horizontal scaling is nominally 2μs/cm in Figures 16-18 and 5 μs/cm in Figure 19. The lower trace in all four

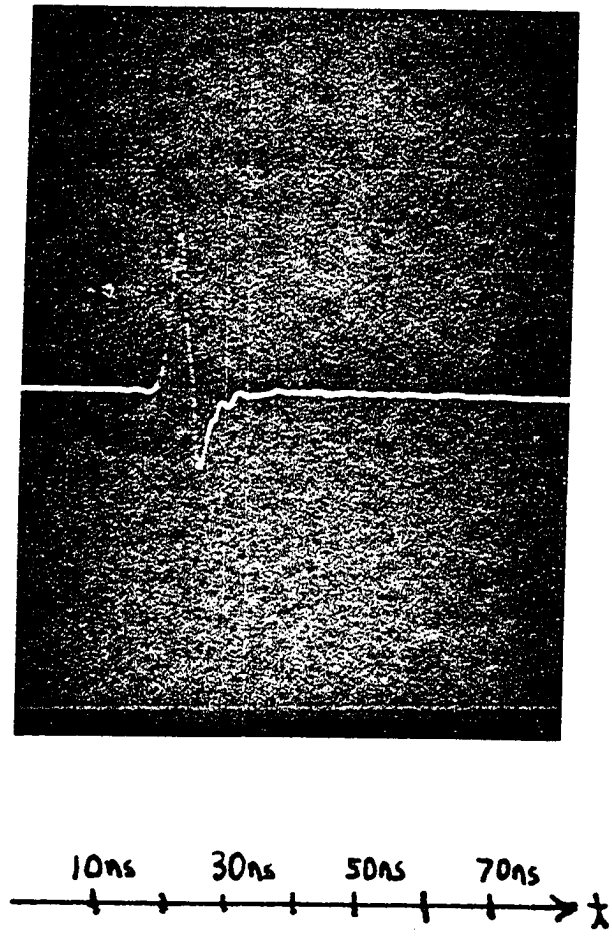

Figure 15. Reflection of pulse as observed on sampling oscilloscope

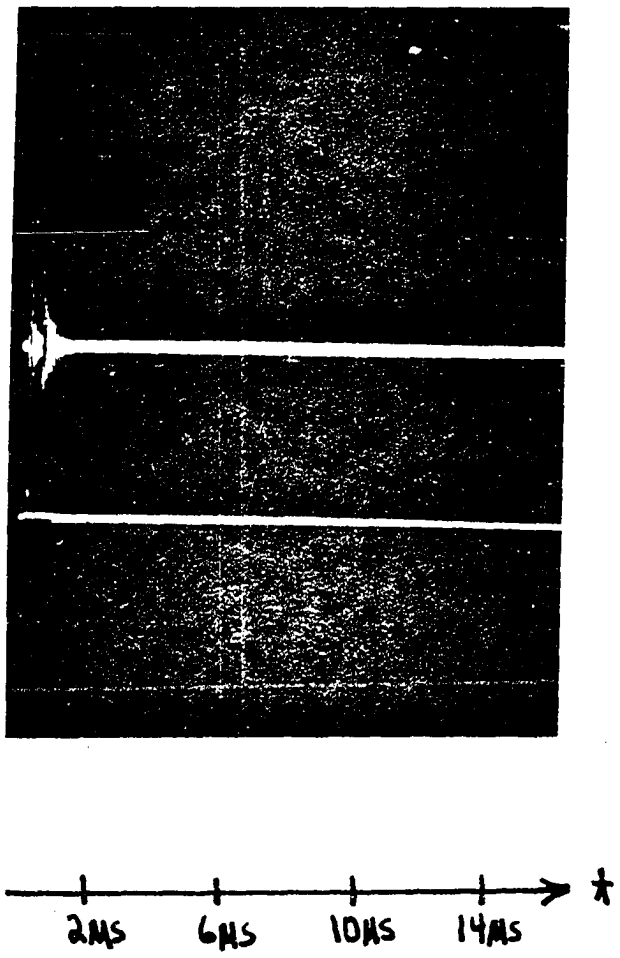

Figure 16. Signal observed when transducer is replaced by short

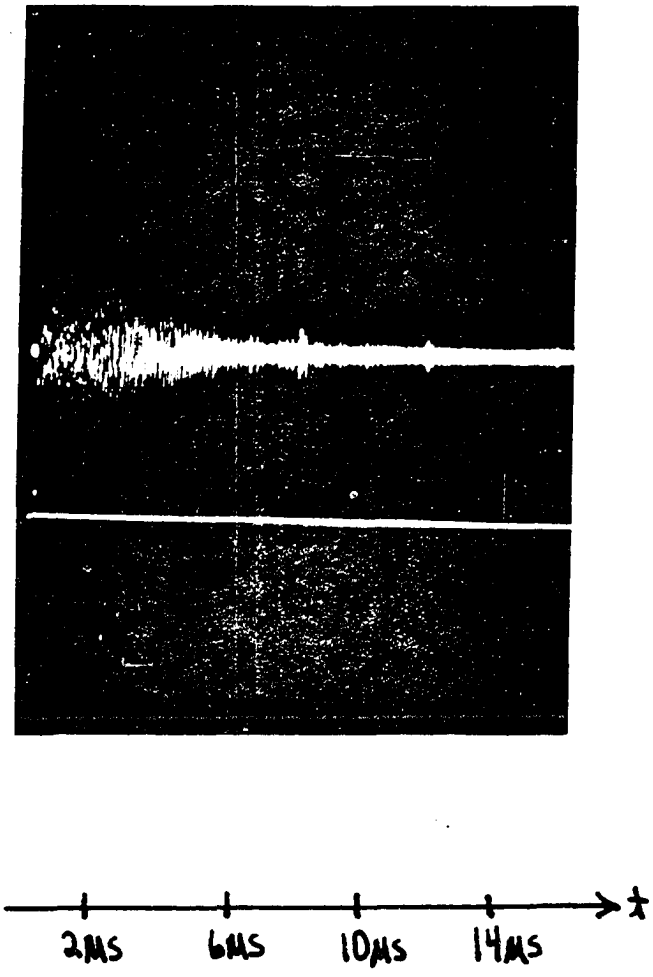

Figure 17. Acoustic return from transducer when excited by 2ns pulse

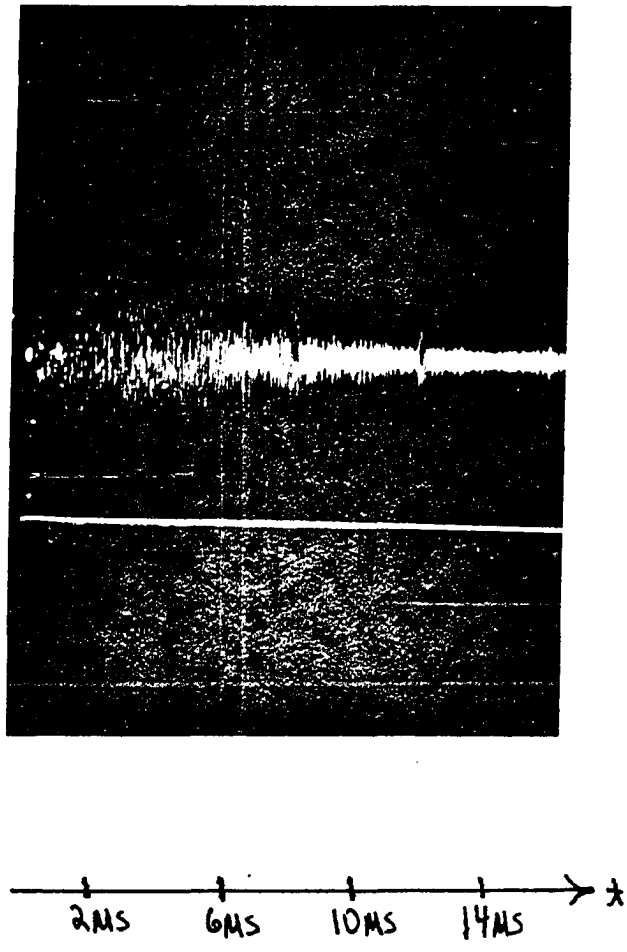

Figure 18. Acoustic return from transducer when excited by 6ns pulse

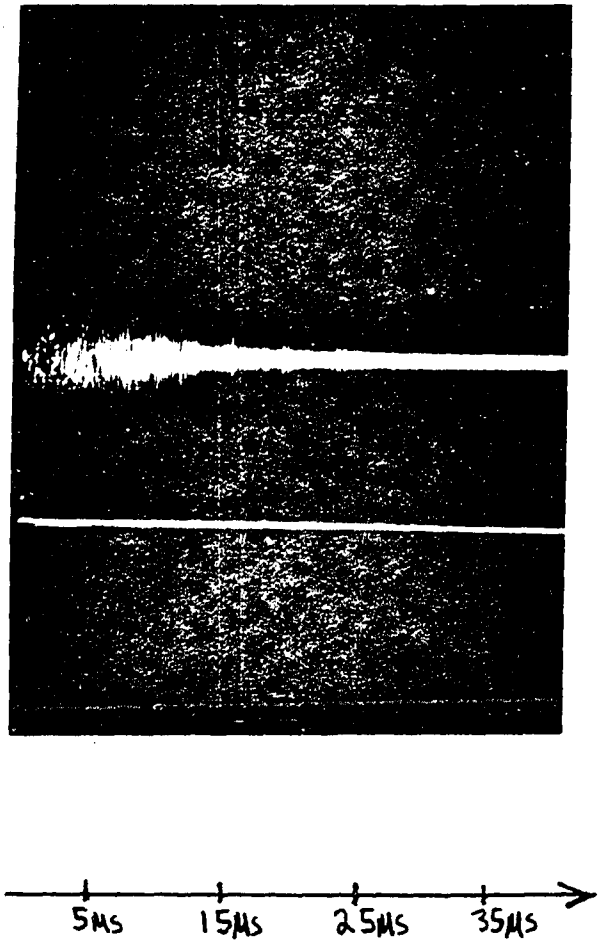

Figure 19. Acoustic return from transducer when excited by 10ns pulse

figures is to nominally indicate the point in time that the voltage pulse is initiated.

In Figure 16 the transducer is replaced by a short. It indicates how well the amplifier recovers from an initially large pulse. The input pulse had a duration of 10ns. It is apparent that signal occurring more than 1 μs after the initial pulse cannot be attributed to amplifier saturation.

Figures 17-19 show the return from the transducer for for 2ns, 6ns, and 10ns pulses respectively. It is noted that a return can be observed for up to 20 μs with the 2ns and 6ns pulses and up to 30 μs with the 10ns pulse. Attention is called to the spikes occurring in a regular fashion on the right hand side of the trace in Figures 17 and 18. At least three of these can be observed. Likewise in Figure 19 beginning slightly right of center and going to the left, four regularly spaced spikes can be observed. A more careful determination of their spacing using a crystal oscillator as the base to calibrate the time scale on the oscilloscope indicates that these spikes are separated by 3.4 μs.

It is also noted that shorting the transducer at the point that contact is made to the stripline causes the extensive post 1 μs signal to disappear. Shielding the device with aluminum foil causes no change in the observed signal. Varying the pulse repetition frequency from 20kHz to 1MHz has little apparent effect on the signal. Touching the surface of the transducer with a camel hair brush changes the post 1 μs signal slightly.

D. Interpreting the Experimental Results

The basal plane strip line model developed in Chapter II and modeled in Figure 12 assumes the excitement of a uniform T.E.M. wave and a longitudinal mechanical wave that are continuously coupled together and contained in the region of the strip line. Theoretically this mode has infinite bandwidth, but it can be expected that lower frequencies will not meet the assumption of uniformity and the actual wave excited could be more complicated than the simple mode envisioned above. Also it is likely that in attempting to bounce the beam off an end of the bar, the upper frequencies will be limited by how well this end is prepared. Therefore, it is to be expected that when a broadband signal such as a short duration pulse is introduced onto the strip line structure, the acoustic return will contain those frequency components of the initial pulse that the transducer can handle and the return pulse will be dispersed. In addition, the method of observation gives a 8 MHz window centered at 30 MHz which introduces dispersion in the observation.

There can be little doubt that the post 1 μs signal shown in Figures 17-19 is acoustic in nature. The experimental procedure outlined in Section C is fairly convincing evidence that the post 1 μs signal is an acoustic return.

There is a possibility that the acoustic return observed in Figures 17-19 is a resonance where the wave motion is perpendicular to the plate (a thickness resonance). The author feels this is unlikely for even given that the mode of operation here is not the manner in which a thickness mode would be excited, the fact that the return is fairly independent

of the pulse repetition frequency would seem to be strong evidence that the thickness resonance is not excited.

The spikes in the acoustic return that are separated by 3.4 μs are fairly strong evidence that at least in that part of the return the observed signal is indeed the strip line mode mentioned above. The strong signal immediately following the input pulse could be understood as multiple reflections between the near end of the bar and the point of excitation. That is, the model of Figure 12 predicts pulses leaving in both directions. The return spikes every 3.4 μs can be understood as reflections from the far end of the bar. The hash preceding these spikes may be understood as reflections from the near end of the bar which are in turn reflected by the point of excitation as predicted by the model of Figure 12. This near signal may be understood, then, as a pulse bouncing between the near end of the bar and the point of excitation. With every bounce, part of its energy is leaked out the transformer or down the other side of the bar to the far end.

IV. SUMMARY AND CONCLUSIONS

A microwave frequency bulk wave transducer scheme has been suggested in this thesis. Basically the scheme involves construction of strip lines on piezoelectric crystals of the correct symmetry and orientation. The specific case investigated was propagation in the basal plane or along the c axis for crystals of 4mm symmetry. It was shown that the modes excited could be regarded as two capacitively coupled transmission lines where one line corresponds to the electromagnetic wave and the other the acoustic wave. A power series approximation technique was developed to analyze the class of problems that arise for this structure. It was shown that shorting the electric field on one or both ends of the line caused acoustic waves moving in only one direction in the transducer region. This kind of transducer is not mechanically resonant. It is felt that this property should greatly facilitate mechanical fabrication for use at higher frequencies. It is also shown that when the ends of the electrical line are shorted, the acoustic and electric lines may be regarded as uncoupled except for a transformer at the point of excitation. It is also indicated that these transducers may be located at will on the piezoelectric substrate. Estimations of insertion loss based on published data for barium titanate are made. It is found that a c axis transducer would be quite attractive.

A transducer was constructed using barium titrate as the piezoelectric material. This transducer was a strip line formed on a bar 1.14 cm long and shorted on one end. The crystal was poled so that

propagation took place in the basal plane. The transducer was excited by a voltage pulse varying in duration from 2ns to 10ns. An acoustic return lasting up to 30 μs could be clearly observed. It is felt that results of this experiment bear out many aspects of the analysis. In particular the decoupled transmission line model mentioned above yielded a consistent interpretation of the experimental data. To the author's knowledge, no transducer has ever been constructed that could handle such short duration pulses.

The capability of being able to arbitrarily locate the transducer on the substrate depends upon being able to short the electric field over the side of the crystal. This concept was not experimentally verified primarily because the crystals at the author's disposal were not long enough.

V. LITERATURE CITED

1. Baranskii, K. N. The excitation of hypersonic frequencies in quartz. Soviet Physics-Doklady 2: 237-238. May 1957.

2. Bommel, H. E. and K. Dransfeld. Excitation of very high frequency sound in quartz. Physics Review Letters 1: 234-236. October 1958.

3. McCue, J. J. G. and R. W. Danion, eds. Special issue on ultrasonics. Proceedings IEEE 53: 1285-1635. October 1965.

4. Bahr, A. J., ed. Special issue on microwave acoustics. IEEE Trans. Microwave Theory and Techniques MTT-17: 799-1040. November 1969.

5. Adler, R. B., L. J. Chu, and R. M. Fano. Electromagnetic energy transmission and radiation. New York, New York, John Wiley and Sons, Inc. 1960.

6. Berlicourt, D. A., D. R. Curran, and H. Jaffe. Piezoelectric and piezomagnetic materials and their function in transducers. In Mason, W. P., ed. Physical acoustics. Vol. IA. Pp. 169-270. New York, New York, Academic Press, Inc. 1964.

7. Kyame, J. J. Wave propagation in piezoelectric crystals. Journal Acoustical Society of America 21: 159-167. May 1949.

8. Kyame, J. J. Conductivity and viscosity effects on wave propagation in piezoelectric crystals. Journal Acoustical Society of America 26: 990-993. November 1954.

9. Hutson, A. R. and D. L. White. Elastic wave propagation in piezoelectric semiconductors. Journal of Applied Physics 33: 40-47. January 1962.

10. Nye, J. F. Physical properties of crystals. London, Oxford Press, Inc. 1957.

11. Mason, W. P. Physical acoustics and the properties of solids. Princeton, New Jersey, D. Van Nostrand Company, Inc. 1958.

12. Louisell, W. H. Coupled mode and parametric electronics. New York, New York, J. Wiley and Sons, Inc. 1960.

13. Reeder, T. M. and D. K. Winslow. Characteristics of microwave acoustic transducers for volume wave excitation. IEEE Trans. Microwave Theory and Techniques MTT-17: 927-941. November 1969.

14. LeCraw, R. C. and R. L. Comstock. Magnetostatic interactions in ferromagnetic insulators. In Mason, W. P., ed. Physical acoustics. Vol. IIIB. Pp. 127-200. New York, New York, Academic Press, Inc. 1965.

15. White, D. L. The depletion layer and other high frequency transducers using fundamental modes. In Mason, W. P., ed. Physical acoustics. Vol. IB. Pp. 321-352. New York, New York, Academic Press, Inc. 1964.

16. De Klerk, J. Fabrication of vapor-deposited thin film piezoelectric transducers for the study of phonon behavior in dielectric materials at microwave frequencies. In Mason, W. P., ed. Physical acoustics. Vol. IVA. Pp. 195-225. New York, New York, Academic Press, Inc. 1966.

17. Mason, W. P. Piezoelectric crystals and their application to ultrasonics. Princeton, New Jersey, D. Van Nostrand Company, Inc. 1950.

18. Carr, P. H. The generation and propagation of acoustic surface waves at microwave frequencies. IEEE Trans. Microwave Theory and Techniques MTT-17: 912-919. November 1969.

19. Stern, E. Microsound components, circuits and applications. IEEE Trans. Microwave Theory and Techniques MTT-17: 835-844. November 1969.

20. Adkins, L. R. and H. J. Shaw. Surface wave delay line amplifiers. IEEE Trans. Microwave Theory and Techniques MTT-17: 912-919. November 1969.

21. Lean, E. G. and A. N. Broers. Acoustic and transferred electron circuits. IEEE International Solid State Circuits Conference Technical Paper Digest 1970: 130-131. 1970.

22. White, D. C. and H. H. Woodson. Electromechanical energy conversion. New York, New York, John Wiley and Sons, Inc. 1959.

23. Thurston, R. N. Wave propagation in Fluids and normal solids. In Mason, W. P., ed. Physical acoustics. Vol. IA. Pp. 2-111. New York, New York, Academic Press, Inc. 1964.

24. Pierce, J. R. Traveling wave tubes. Princeton, New Jersey, D. Van Nostrand Company, Inc. 1950.

25. Ramo, S. and J. R. Whinnery. Fields and waves in modern radio. New York, New York, John Wiley and Sons, Inc. 1953.

26. Benedict, T. S. and J. L. Durand. Dielectric properties of single domain crystals of $BaTiO_3$ at microwave frequencies. Physics Review 109: 1091-1093. February 1958.

27. Lurio, A. and E. Stern. Measurements of the dielectric constant of $BaTiO_3$ single crystals in the paraelectric region at X band. Journal of Applied Physics 31: 1802-1808. October 1960.

28. Nakamura, E. and J. Furuichi. Measurement of Microwave dielectric constants of ferroelectrics. Journal of Physical Society of Japan 15: 1955-1960. November 1960.

29. Berlincourt, D. and H. Jaffe. Elastic and piezoelectric coefficients of single-domain barium titanate. Physics Review 111: 143-148. July 1958.

30. Fatuzzo, E. and W. J. Merz. Ferroelectricity. Amsterdam, North Holland Publishing Company. 1967.

31. Jona, F. and G. Shirane. Ferroelectric crystals. New York, New York, Macmillan Company, Inc. 1962.

32. Warner, R. M. and J. N. Fordemwalt. Integrated circuits. New York, New York, McGraw-Hill Book Company, Inc. 1965.

33. Last, J. T. Preparation of thin single crystals of barium titanate. Review of Scientific Instruments 28: 720-721. September 1957.

VI. ACKNOWLEDGMENTS

Professor A. V. Pohm has greatly aided and encouraged the author during the course of his graduate career.

The author received much useful advice and encouragement from Professor R. E. Post. The author had useful conversations with Mr. T. M. McRoberts and Mr. D. M. Morton. Mr. J. T. McConnell, Mr. D. Flack, and Mr. J. Musil performed machine work that aided various parts of the experimental program. Mr. C. Day and Professor C. S. Comstock aided the author in evaporating the strip lines. Professor J. P. Basart provided electronic instruments that facilitated the measurements. All of the above individuals are associated with the Department of Electrical Engineering, Iowa State University, Ames, Iowa.

The thesis was typed by Mrs. Kathy Lucas.

The author's wife, Gwen, helped in preparation of the manuscript and was very patient during the course of the work reported here.

The Solid State Affiliates Program supported most of the work reported in this thesis.

VII. APPENDIX A

The dual of the electrically resonant transducer analyzed in Chapter II is analyzed here. This structure which will be termed a mechanically resonant transducer (because it will be shown to have no electrical resonance) is indicated schematically in Figure 20. The mechanically resonant transducer (M.R.T.) has no apparent practical application but the phenomena of the uncoupling of the acoustic and electric modes as indicated in Chapter II is so intellectually remarkable that it was thought to be worthwhile to include another example of it here.

The boundary conditions to be applied as indicated in Figure 20 are given below.

$$\hat{V}(-\ell_-) = \hat{V}(\ell_+) = 0 \tag{203}$$

$$\hat{H}_y(0^-) = \hat{H}_y(0^+) \tag{204}$$

$$\hat{E}_x(0^-) = \hat{E}_x(0^+) \tag{205}$$

It is useful to apply the variables $\hat{t}$ and $\hat{h}$ (see Equations 175 and 176) again and for this structure,

$$\hat{h}(\mp\ell_\mp) = \hat{H}_y(\mp\ell_\mp) \tag{206}$$

because it is clamped at $z = \pm\ell_\pm$.

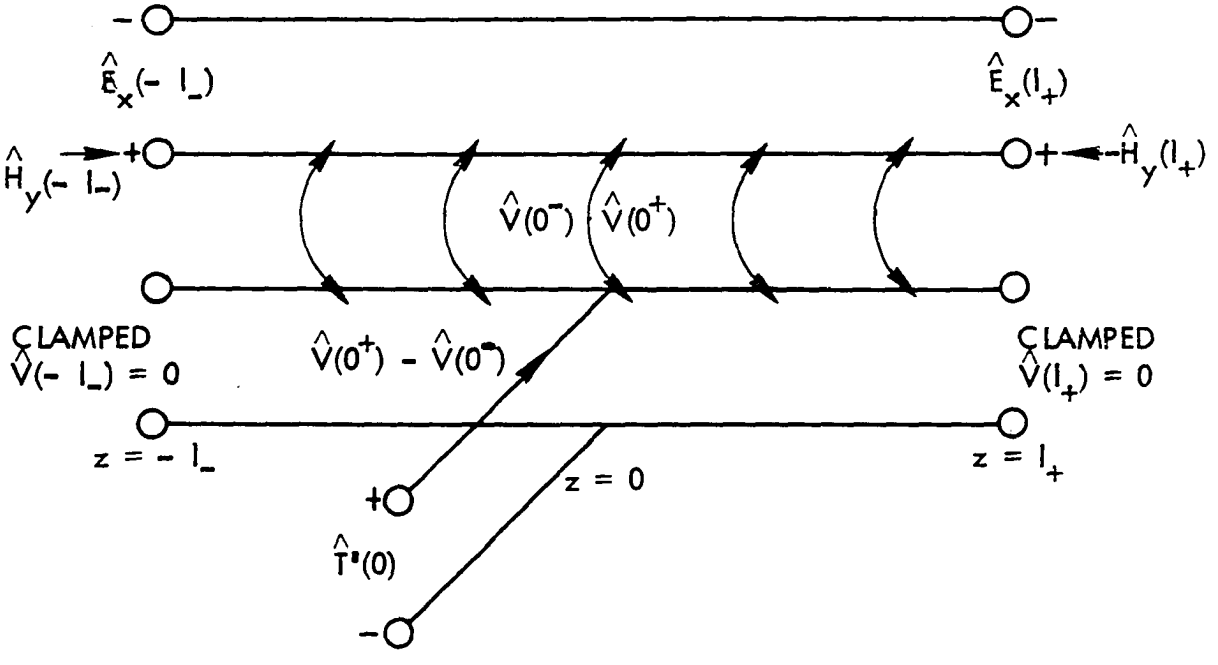

Figure 20. The mechanically resonant transducer

Equation 203 implies (using Equations 148-151)

$$\hat{V}(z) = \hat{V}(0^{\mp}) \frac{\sin\beta_A(l_{\mp} \pm z)}{\sin\beta_A l_{\mp}} \tag{207}$$

$$\hat{I}(z) = \pm j\hat{V}(0^{\mp}) \frac{\cos\beta_A(l_{\mp} \pm z)}{\sin\beta_A l_{\mp}} \tag{208}$$

Equation 204 implies

$$\hat{h}(0^+) - \hat{h}(0^-) = \sqrt{\kappa\delta}\left[\hat{V}(0^+) - \hat{V}(0^-)\right] \tag{209}$$

Equation 205 implies

$$\hat{I}(0^+) - \hat{I}(0^-) = \hat{T}'(0^+) - \hat{T}'(0^-) \tag{210}$$

If the mechanical source at z = 0 were balanced, $\hat{V}(0^-) = \hat{V}(0^+)$, then $\hat{h}(0^+) = \hat{h}(0^-)$ and the two lines would be completely uncoupled. Therefore it is necessary to apply unbalanced excitation as indicated in Figure 20. Therefore

$$\hat{I}(0^-) = \hat{I}(0^+) \tag{211}$$

and

$$\hat{I}(0) = \hat{T}'(0) - \sqrt{\kappa\delta}\,\hat{E}_x(0) \tag{212}$$

Of course

$$\hat{E}_x(z) = \hat{E}^+_{\mp} e^{-j\beta_E z} + \hat{E}^-_{\mp} e^{+j\beta_E z} \tag{213}$$

and

$$\hat{h}(z) = \sqrt{1-\kappa}\left[\hat{E}^+_{\mp} e^{-j\beta_E z} - \hat{E}^-_{\mp} e^{+j\beta_E z}\right] \tag{214}$$

It is found that

$$\frac{\hat{T}'(0)}{\hat{V}(0^+) - \hat{V}(0^-)} + \frac{\kappa\delta}{\left(\hat{h}(0^-)/\hat{E}_x(0)\right) + \left(-\hat{h}(0^+)/\hat{E}_x(0)\right)} = \frac{1}{j\tan\beta_A \ell_+ + j\tan\beta_A \ell_-} \tag{215}$$

The ratios $\hat{h}(0^-)/\hat{E}_x(0)$ and $-\hat{h}(0^+)/\hat{E}_x(0^+)$ are related to $\hat{H}_y(-\ell_-)/\hat{E}_x(-\ell_-)$ and $-\hat{H}_y(\ell_+)/\hat{E}_x(\ell_+)$ by the well known transmission line translations implied by Equations 213, 214 and 206.

Equations 207-209 and 212-215 imply that the three accessible ports of the M.R.T. can be understood by the circuit model of Figure 21. The uncoupling of the modes except for the transformer at z = 0 is again observed.

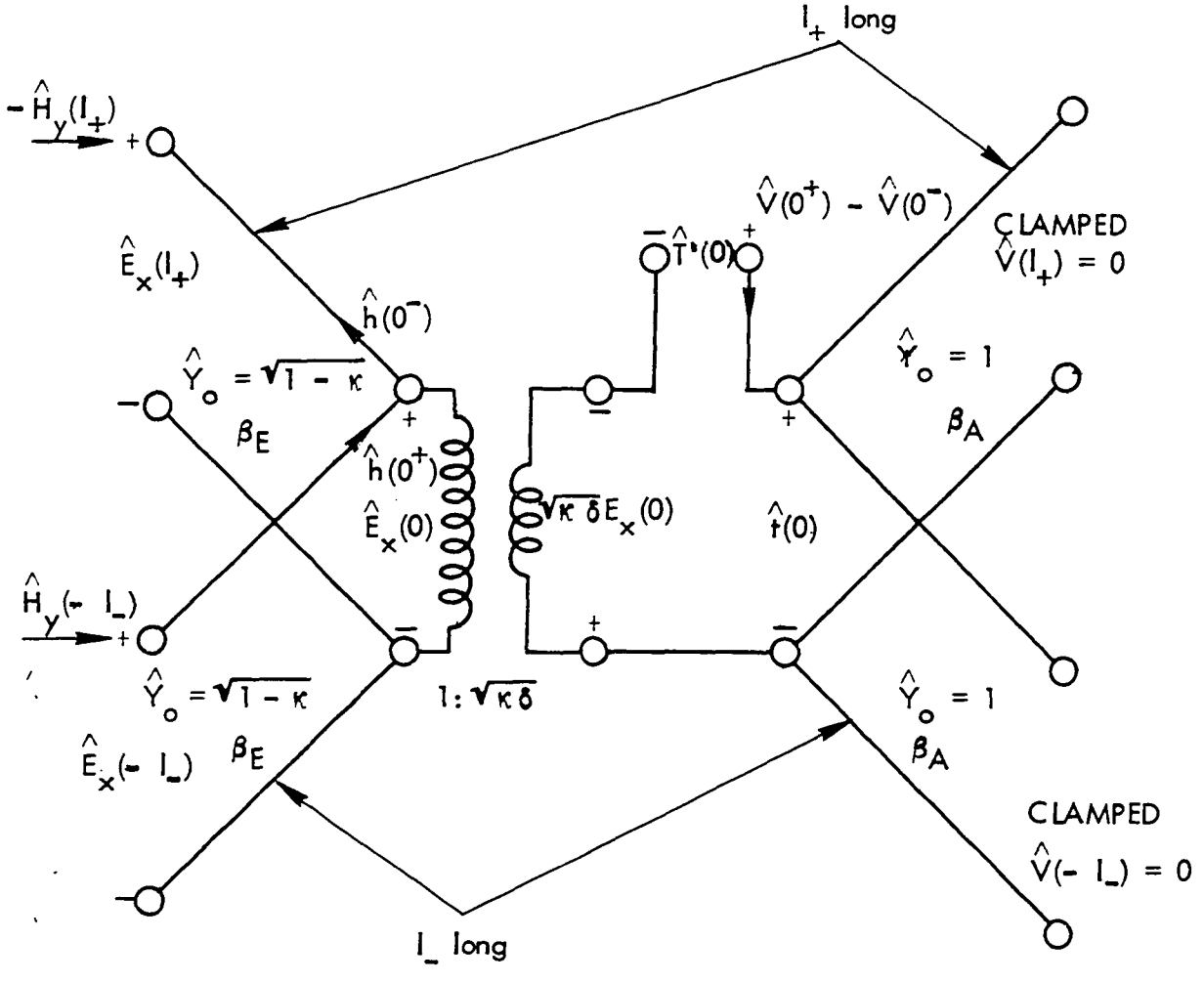

Figure 21. Model showing behavior of M.R.T. at its accessible ports

VIII. APPENDIX B

A quasi-static transducer using the one-dimensional model of Chapter II, Section D is considered. This is a standard calculation and is reviewed here in order that the results can be compared to the E.R.T. of Chapter II.

The problem to be considered is schematically indicated in Figure 22. It is assumed that $\ell << \lambda_E$ and that Equations 152-155 using the quasi-static approximation can be employed. The boundary conditions for the structure of Figure 22 are as below.

$$\hat{H}_y(\ell) = 0 \tag{216}$$

$$\hat{T}'(0) = -\hat{R}_1 \hat{V}(0) \tag{217}$$

$$\hat{T}'(\ell) = \hat{R}_2 \hat{V}(\ell) \tag{218}$$

Substitution of Equations 218-220 into Equations 152-155 readily yields the following.

$$\hat{Y}_{in} = \hat{H}_y(0)/\hat{E}_x(0) = j\beta'_{EE}(1-K)\ell + \hat{g}_A + j\hat{b}_A \tag{219}$$

$$\hat{g}_A = SK \frac{(\hat{R}_1+\hat{R}_2)(1-\cos\theta)\left[\hat{R}_1\hat{R}_2(1+\cos\theta)+(1-\cos\theta)\right]}{(1+\hat{R}_1\hat{R}_2)^2\sin^2\theta + (\hat{R}_1+\hat{R}_2)^2\cos^2\theta} \tag{220}$$

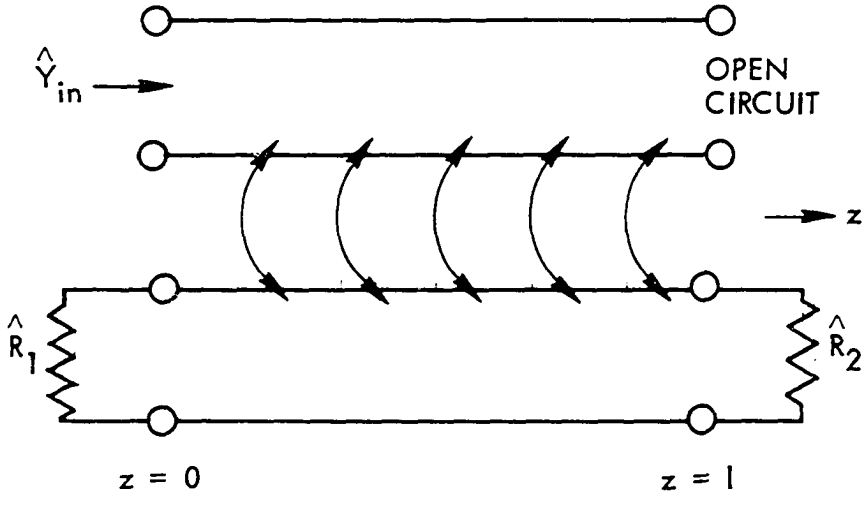

Figure 22. Schematic representation of a quasi-static transducer

$$\hat{b}_A = \frac{\delta K \sin\theta \left[2(1+\hat{R}_1\hat{R}_2)(1-\cos\theta) + (\hat{R}_1+\hat{R}_2)^2\cos\theta \right]}{(1+\hat{R}_1\hat{R}_2)^2 \sin^2\theta + (\hat{R}_1+\hat{R}_2)^2\cos^2\theta} \quad (221)$$

$$\theta = \beta'_{AA}\, l \quad (222)$$

Consider the practical case where

$$\hat{R}_1 = 0 \quad (223)$$

$$\hat{R}_2 = 1 \quad (224)$$

Then

$$\hat{q}_A \Big|_{\substack{\hat{R}_1=0 \\ \hat{R}_2=1}} = \delta K (1-\cos\theta)^2 \quad (225)$$

$$\hat{b}_A \Big|_{\substack{\hat{R}_1=0 \\ \hat{R}_2=1}} = \delta K \sin\theta \left[2-\cos\theta \right] \quad (226)$$

Resonance corresponds to $l = \lambda'_{AA}/2$ and

$$\hat{g}_A \Big|_{\substack{\hat{R}_1=0 \\ \hat{R}_2=1 \\ \ell=\lambda'_{AA}/2}} = 4\delta K \tag{227}$$

$$\hat{b}_A \Big|_{\substack{\hat{R}_1=0 \\ \hat{R}_2=1 \\ \ell=\lambda'_{AA}/2}} = 0 \tag{228}$$

It is apparent by comparing Equation 227 to Equation 165, that g_A at mechanical resonance is only four times greater than Y_{in} for the E.R.T. located on the end of stress free bar. This is why they were said to be comparable. Of course the E.R.T. is not mechanically resonant.

The situation somewhat analogous to the arbitrarily located E.R.T. is to let $\hat{R}_1 = \hat{R}_2 = 1$. Then

$$\hat{g}_A \Big|_{\hat{R}_1=\hat{R}_2=1} = \tfrac{1}{2}\delta K(1-\cos\theta) \tag{229}$$

$$\hat{b}_A \Big|_{\hat{R}_1=\hat{R}_2=1} = \delta K \sin\theta \tag{230}$$

Resonance corresponds to $\ell = \lambda'_{AA}/2$ and

$$\hat{g}_A \Big|_{\substack{\hat{R}_1 = \hat{R}_2 = 1 \\ \ell = \lambda'_{AA}/2}} = 5K \tag{231}$$

$$\hat{b}_A \Big|_{\substack{\hat{R}_1 = \hat{R}_2 = 1 \\ \ell = \lambda'_{AA}/2}} = 0 \tag{232}$$

Comparing Equation 231 to Equation 178, it is seen that this conductance is twice as big as the arbitrarily located E.R.T. at electrical resonance.